TRR
JOURNAL OF THE TRANSPORTATION RESEARCH BOARD

Research Article

Transportation Research Record
2023, Vol. 2677(5) 966–990

DOI: 10.1177/03611981221138511
journals.sagepub.com/home/trr
SAGE

Modified Bureau of Public Roads Link Function

Ninad Gore[1], Shriniwas Arkatkar[1], Gaurang Joshi[1], and Constantinos Antoniou[2]

Abstract

The Bureau of Public Roads (BPR) function is a widely used link cost function in transportation planning because of its simple mathematical form, easily measurable field variables, and consistent performance. However, the BPR function is deterministic and does not capture the stochastic relation between travel time and traffic flow. The present study develops a modified BPR (MBPR) function by incorporating travel time uncertainty (TTU) in the deterministic BPR function. In the MBPR function, the effect of TTU is incorporated using two parameters, γ and δ. A nonlinear optimization problem is formulated, and the generalized reduced gradient method is used to calibrate the BPR and the MBPR function. The applicability of the proposed MBPR function is demonstrated using empirical data collected for an urban arterial in India and simulated data developed for a real-world urban road network. The proposed MBPR function captures the heterogeneity in travel time for different traffic flow values. The function (a) captures the variability in travel time under oversaturated conditions and (b) captures the time-dependent relation between traffic volume and delay. The physical meaning of γ and δ in the context of inter-day heterogeneity, infrastructure potential, and traffic flow heterogeneity are discussed. The practical application of MBPR as an analytical tool for system-wide performance evaluation is demonstrated by investigating the impact of traffic signal control on travel times using a before–after perspective. Compared with the before case, a 13% reduction in travel time is observed for the after case. Therefore, the installation of traffic signal control has reduced congestion.

Keywords

highway capacity and quality of service, arterials, microscopic traffic simulation, traffic flow theory and characteristics, macroscopic traffic models

The link cost function plays a vital role in transportation planning applications as it explains the variation in travel times along the segment as a function of link volume. A typical link cost function should consider free-flow travel time, link delay, and intersection delays in its formulation. The Bureau of Public Roads (BPR), Davidson's, Akcelik's, and conical delay functions are the most commonly used link cost functions. The BPR function has profound applications in transportation planning primarily as a result of its simple mathematical form, easily observable field inputs, and consistent performance (*1*, *2*).

The BPR function is formulated as a polynomial function with respect to the ratio of traffic volume to capacity. The alpha (α) and beta (β) are parameters of the BPR function and, thus, represent the performance of a network (*3*). The α is the scale parameter; the β is the shape parameter, and its value varies between cities. The parameter of BPR function α is the ratio of travel time per unit distance at practical capacity to the free flow, and parameter β determines how fast the curve increases from the free-flow travel time (*4*). Generally, $\alpha = 0.15$ and $\beta = 4$ are used. A higher value of β indicates that the onset of congestion becomes more and more sudden (*5*).

Manzo et al. (*6*) argued that the BPR function may be suitable only when the traffic flow is below capacity ($V/C < 1$). For $V/C > 1$, the BPR function was observed to

[1]Department of Civil Engineering, Sardar Vallabhbhai National Institute of Technology (SVNIT), Surat, India
[2]Transportation Systems Engineering, Technical University of Munich, Germany

Corresponding Author:
Shriniwas Arkatkar, sarkatkar@gmail.com

overpredict the average speed (*7*). For the links with flow far below the capacity, especially when the values of α are very high, the function always yields free-flow times independent of the actual flow on the link (*5*, *8*). Huntsinger and Rouphail (*9*) reported that bottleneck analysis and queue length estimation effectively provide a valuable tool for improving volume–delay functions (VDFs) with locally collected data. Wong and Wong (*10*) correlated the topological network metrics and the macroscopic Bureau of Public Roads (MBPR) function parameters. Free-flow travel time and congestion sensitivity parameters of the MBPR function were correlated with the average number of junctions per unit distance and the road density. The BPR function does not consider traffic control and roadway-based parameters, forming its major drawback (*7*). The BPR function is crucial in static user equilibrium analysis (*11*). Researchers in the past calibrated the VDFs precisely, the BPR function, to develop traffic assignment and travel demand models (*1*, *12–14*). Further, the BPR function was also adopted to develop combined trip distribution and assignment models (*15*), mixed traffic equilibrium models integrating mode, route, and transfer choices under logit based framework (*16*), optimization of transit road space priority at the network level (*17*), and evaluation of the price of anarchy in the network (*18*).

Research Motivation

Researchers have widely used the BPR function for transportation planning purposes. It can be noted that most studies are carried out for homogeneous traffic conditions. However, limited studies have calibrated the BPR function under heterogeneous traffic conditions prevailing in India (*19*, *20*).

Traditionally, most traffic flow models are deterministic because they are theoretically and computationally traceable. However, traffic flow on urban networks is highly stochastic and random because travelers make unpredictable decisions. The random characteristics of traffic flow are attributed to the interaction between (a) vehicles with diverse static and dynamic properties, (b) diverse drivers with different perceptions, responses and driving habits, (c) frustration, and (d) roadway and traffic control features. This random nature of traffic flow leads to stochastic values of travel time, thereby giving rise to uncertainties in travel time. The uncertainties in travel time significantly affect travelers' frustration and scheduling of trips. Therefore, without accounting for the heterogeneity in traffic flow, the deterministic traffic flow models and link cost functions limit their capacity to represent traffic flow practically and may result in inaccurate or misleading results in modeling traffic control strategies. The traffic flow on the urban network and corridors is highly dynamic and rarely is in a steady state. The variation in roadway geometry and traffic control characteristics over space creates a wide variation in traffic flow. The existing BPR function is deterministic and does not effectively capture the stochastic travel time to traffic flow relation. However, to the best of the authors' knowledge, no studies have examined the effect of travel time uncertainty (TTU) on the performance of the BPR function and subsequently developed a modified BPR (MBPR) function by incorporating TTU.

The present study proposes an MBPR created by incorporating TTU in the existing deterministic BPR function. In the MBPR function, the effect of TTU is incorporated using two parameters, γ and δ. The physical meaning of these parameters in the context of inter-day heterogeneity, infrastructure potential, and traffic flow heterogeneity is explained. The applicability of the proposed MBPR function is demonstrated using empirical data collected for an urban arterial in India and simulated data developed for a real-world urban road network. Based on the investigations, it is concluded that the proposed MBPR function can capture the heterogeneity in travel time for a specific value of traffic flow very well and therefore is stochastic. The contributions of the proposed MBPR function are twofold: (a) quantifying the effect of TTU on travel time and (b) incorporating TTU in the existing BPR function to capture the heteroskedastic relation of travel time to traffic flow.

The remainder of the manuscript is organized into four sections. The following section explains the methodology adopted for developing the MBPR function. The physical meaning of γ and δ parameters and calibration methodology are explained in the "Methodology" section. The section titled "Data" briefly introduces the data, followed by simulation modeling. The estimation of the fundamental diagram (FD) and macroscopic fundamental diagram (MFD) using empirical and simulated datasets is subsequently explained. The performance of the BPR and MBPR function for both empirical and simulated datasets and the physical meaning of γ and δ are discussed in the "Results and Discussions" section. The practical application of the MBPR function is also discussed in the "Results and Discussion" section. The final sections give the conclusion.

Methodology

Bureau of Public Roads Function

The BPR function, as given by Pan et al. (*21*) and Qiu et al. (*22*), is represented as

$$T_a = t_f\left(1 + \alpha \times \left(\frac{Q_a}{C_a}\right)^{\beta}\right) \quad (1)$$

where

T_a = travel time of road segment (s);

t_f = free-flow travel time (s);

Q_a = average traffic flow on road segment (vehicles per hour [vph]);

C_a = capacity of road segment (vph); and

α and β = model parameter.

The boundary condition of the BPR function can be represented as follows.

For $Q_a = 0$

$$T_a = t_f, \quad (2)$$

For $Q_a = C$

$$T_a = t_f \times (1 + \alpha). \quad (3)$$

The above formulation has known drawbacks. First, the BPR function performs well in free-flow and congested states (broadly undersaturated conditions). However, the BPR function cannot represent the oversaturated conditions—that is, it cannot capture phenomena like queue buildup, queue dissipation, and queue spillover. For the BPR function to represent the oversaturated conditions, it is argued that a modified volume or "oversaturated" demand (capacity volume plus the residual queue) should be used (*9*). Second, the BPR function presented in Equation 1 does not capture the time-dependent relation between traffic volume, travel time, and delay. Finally, the formulation is deterministic. However, the changes in travel time under similar traffic flow conditions vary significantly with different circumstances (*23*). This highlights that the relationship between travel time and traffic flow is stochastic. The drawbacks mentioned above warrant the development of an MBPR. Ideally, the MBPR function should (a) represent oversaturated conditions, (b) explain the time-dependent relation between traffic flow and travel time, and (c) capture the stochastic relation between traffic flow and travel time.

Modified BPR Function

Travel time is the travel distance over the travel speed; therefore, examining the speed–flow relationship can help better understand the travel time–flow relation. It is well-known that a wide variation exists in the speed–flow relationship (*24*). The wide scatter of the speeds or travel times for a given flow can be broadly attributed to two factors:

(a) The variation in speed or travel time for a specific traffic flow value could indicate that the observations may belong to different traffic states (free-flowing, more or less congested, or congested conditions).

(b) The variation in speed or travel time for a given traffic state (i.e., free-flow, more or less congested, or congested condition) can also be attributed to the uncertainty of the speeds/travel times.

Therefore, for understanding the wide variation in travel time or speed with traffic flow, it is essential to consider that the traffic can be in different states, and, more importantly, that the magnitude of TTU for a given traffic flow condition can also induce variation in travel times or speeds. From this simple analysis, it can be inferred that travel times are influenced by the traffic flow and the magnitude of TTU for the given value of traffic flow.

The present study adopted the difference between 90th percentile and 10th percentile travel time at a given traffic flow level to measure TTU (*25*). Mahmassani et al. (*26*) and Yildirimoglu et al. (*27*) proposed standard deviation and interquartile range to measure TTU. Therefore, the definition of TTU proposed by Mahmassani et al. (*26*) and Yildirimoglu et al. (*27*) could also be used.

Higher TTU values indicate that travel times are uncertain for a given traffic flow condition. The TTU, as proposed by Tu et al. (*25*), is given as

$$\text{TTU(s/km)} = \left(\frac{T_{90} - T_{10}}{l_r}\right) \quad (4)$$

where T_{90} = 90th percentile travel time, T_{10} = 10th percentile travel time, and l_r = length of route.

The percentile-based measures have several practical advantages. First, their statistical properties are more robust than mean, standard deviation, or other moment-based indicators. Here, the meaning of "robust" in a statistical context reflects that since the travel time distribution is either left- or right-skewed, the value of the mean, standard deviation, and other moment-based indicators will be sensitive to outliers, and therefore percentile-based measures are used. Second, the statistic defined is normalized per unit space, which allows its comparison with links of different lengths. Third, interpretation becomes simple. The TTU calculated using Equation 4 can be interpreted "as the expected amount of travel time variation (seconds) per km travel for a given inflow" (*24*).

TTU results from two primary sources. From the demand side, uncertain traffic flow causes uncertain travel time (based on the assumption that travel time depends on link density or volume). TTU can also result from the supply side as a result of recurrent factors (such as the variation in traffic composition on different days,

lane changes, control characteristics, driver perception, driving habits) and non-recurrent factors (like incidents and environmental factors) (*28*, *29*). It is expected that TTU proposed by Tu et al. (*25*) would capture the effect of both the demand- and the supply-side factors.

Model Development

Travel time as traffic flow and TTU can be expressed as a multivariate function, as shown in Equation 5.

$$T = f(Q, \mathrm{TTU}(x,t)) : \left(\mathbb{R}^+, \mathbb{R}, \mathbb{R}^+, \Omega\right) \mapsto \mathbb{R}^+ \tag{5}$$

where f is a real-valued continuous function defined on a real space $\mathbb{R}$. Here, TTU is the randomness component for a given value of Q, defined as a set of real numbers in the domain of Ω. Ω is the probability space equipped with a measure $P_{x,t}(\cdot)$.

Equation 5 suggests that the travel time along the road segment is a function of traffic flow and TTU. Including x and t enables us to model inhomogeneous roads and time-varying conditions like road accidents. So, when Q, x, and t are fixed, travel time is influenced by the value of TTU.

Ngoduy (*30*) and Li et al. (*31*) reported that TTU significantly affects free-flow conditions, especially free-flow travel time. Therefore, the free-flow travel time for the proposed MBPR function is defined as

$$t_f{}^d \equiv t_f{}^s \times \theta \tag{6}$$

where $t_f{}^s$ = free-flow travel time for the stochastic model, $t_f{}^d$ = free-flow speed for the deterministic model, and θ = the stochastic induction factor.

The factor θ would induce a stochastic variation in travel time at a given level of traffic flow based on values of TTU and, therefore, would account for the heterogeneity in the travel time–traffic flow relation. Based on the value of $t_f{}^d$ and θ, the domain of the travel time for the stochastic model can be written as

$$T = \left[t_f{}^s, t_{\max}\right] \tag{7}$$

where $t_{\max}$ = maximum travel time, which would be dependent on the value of Q and TTU.

If the TTU is high, the travel time under free-flow conditions can be higher than the free-flow travel time and vice-versa. However, the values of $t_f{}^s$ should be bounded as one can accidentally compute relatively low travel time, which otherwise is impossible. Therefore, a numerical boundary condition on the $t_f{}^s$ is introduced, which is represented as

$$T_{\min} < t_f{}^s < f(Q, \mathrm{TTU}) \tag{8}$$

where $T_{\min}$ = minimum possible travel time between the segments. Note that this value should be defined in an empirical context.

The stochastic induction factor (θ) is defined as a power function based on the value of TTU for a given traffic flow.

$$\theta = \gamma \times (\mathrm{TTU})_q{}^{\delta} \tag{9}$$

where γ and δ are the non-negative model calibration parameters. γ is the travel-time variation sensitivity parameter expressed as kilometers per second. Note that both γ and δ absorb the effect of TTU corresponding to a given value of traffic flow to generate varying travel time values. It should be noted that the value of TTU would govern the value of γ and δ. For a given traffic flow, a higher value of γ and δ indicates that traffic flow is uncertain compared with lower values of γ and δ. Further, it is essential to note that for a similar value of Q, TTU, α & β, a higher value of γ and δ would result in a higher value of travel time compared with lower values of γ and δ. The physical interpretation of γ and δ is explained in detail in the following subsection.

Therefore, the free-flow travel time for the MBPR function is defined as

$$t_f{}^d \equiv t_f{}^s \times \left(\gamma \times (\mathrm{TTU})_q{}^{\delta}\right). \tag{10}$$

The above formulation is incorporated into the existing deterministic BPR function. Thus, substituting for $t_f{}^d$ in Equation 1 yields

$$T(Q, \mathrm{TTU})_a = t_f{}^s \times \left(\gamma \times (\mathrm{TTU})_q{}^{\delta}\right) \times \left[1 + \alpha \times \left(\frac{Q_a}{C_a}\right)^{\beta}\right]. \tag{11}$$

Rearranging Equation 11 gives

$$T(Q, \mathrm{TTU})_a = t_f{}^s \times \left[1 + \alpha \times \left(\frac{Q_a}{C_a}\right)^{\beta}\right] \times \left(\gamma \times (\mathrm{TTU})_q{}^{\delta}\right). \tag{12}$$

Equation 12 expresses travel time as a multivariate function of traffic flow and TTU. The coefficient $\left(\gamma \times (\mathrm{TTU})_q{}^{\delta}\right)$ induces variability in the travel time for a given traffic flow based on the values of TTU. Therefore, the stochastic nature of the travel time–traffic flow relation can be preserved. It should be noted that the values of both γ and δ would also govern the values of travel time in addition to α and β for similar values of Q and TTU.

Properties of the MBPR Function

For $Q_a = 0$

$$T_a = t_f \times \left(\gamma \times (\mathrm{TTU})_q^{\ \delta}\right). \tag{13}$$

For $Q_a = C$

$$T_a = t_f \times (1 + \alpha) \times \left(\gamma \times (\mathrm{TTU})_q^{\ \delta}\right) \tag{14}$$

From Equation 13, it is clear that for $Q_a = 0$, the travel time is a function of TTU. Based on the values of TTU, travel time can be either greater or less than free-flow travel time. However, if significantly lower travel times, which are not feasible, are observed, then, under such cases, the minimum allowable travel time ($T_{\min}$) should be considered. It should also be noted that the BPR function can be derived from MBPR by setting $\gamma = 1$ and $\delta = 0$. Therefore, the MBPR can be rendered a generalized form of the BPR function.

As discussed earlier, TTU is a function of both demand and supply. For instance, the variation in TTU for a constant supply can be attributed to variation in demand or observed volume. Similarly, for constant demand, the variation in TTU could also be attributed to constant changes in the supply or capacity of arterials or networks as a result of traffic control (type of intersection and its characteristics, that is, red time, cycle time, green time for signalized intersections) and roadway geometry (number of lanes). Therefore, TTU inherently accounts for the changes in demand and supply; by incorporating TTU in the BPR function, the variations in travel time caused by changes in demand and supply are captured.

Physical Interpretation of γ and δ

The physical interpretation of γ and δ is explained as follows.

The first interpretation is that the values of γ and δ are indicators of the magnitude of TTU. A higher value of γ and δ for a particular link or a day would indicate higher uncertainties in travel times. γ and δ values, when compared between links or between different days for a particular link, can explain the inter-day heterogeneity in travel times and its variability. The second interpretation is that for the same values of TTU, Q, α, and β, higher γ and δ would yield higher travel time compared with lower values of γ and δ. This means the γ and δ can capture the potential effect of different factors from both the demand and the supply side on travel time and congestion. In the present paper, such effects are summarized as infrastructure potential. A smaller value of γ and δ would indicate that the infrastructure can produce stable and certain travel times and, thus, indicate that the infrastructure is used more efficiently. The third interpretation is that a higher value of γ and δ would indicate that the traffic flow is unstable, that is, the distribution of traffic flow over density is heterogeneous. The "Results and Discussion" section considers these interpretations using empirical and simulated data.

Calibration of BPR and MBPR Function

A nonlinear optimization technique was adopted to calibrate the BPR and the MBPR function. The objective function is defined as minimizing the sum of the squared deviations.

$$\min Z = \sum \left(x_0 - x_p\right)^2 \tag{15}$$

where x_o = observed value and x_p = predicted value.

For the BPR function,

$$\min Z = \sum \left[t_0 - \left[t_f \times \left(1 + \alpha \times \left(\frac{Q_a}{C_a}\right)^{\beta}\right)\right]\right]^2 \tag{16}$$

subject to constraints (STC)

$$\begin{cases} t_f = \text{field observed value} \\ C_a = \text{derived from FD or MFD} \\ \alpha, \beta, t_0, C_a \geq 0 \end{cases}. \tag{17}$$

For the MBPR function,

$$\min Z = \sum \left[t_0 - \left[\begin{array}{c} t_f \times \left(1 + \alpha \times \left(\frac{Q_a}{C_a}\right)^{\beta}\right) \\ \times \left(\gamma \times (\mathrm{TTU})_q^{\ \delta}\right. \end{array} \right] \right]^2 \tag{18}$$

subject to constraints (STC)

$$\begin{cases} t_f = \text{field observed value} \\ C_a = \text{derived from FD or MFD} \\ \alpha, \beta, t_0, C_a, \gamma, \delta \geq 0 \end{cases} \tag{19}$$

where FD and MFD represent the fundamental diagram and macroscopic fundamental diagram.

In the present study, t_f and C_a represent free-flow travel time and capacity, respectively, and were fixed for calibrating the BPR and the MBPR function. This was done to derive a more robust fit (*32*). The travel-time data for low flow conditions (early morning hours) were filtered, and the 15th percentile travel time of the data was computed and denoted as free-flow travel time (*33*). A generalized polynomial function was fitted to the flow–density scatter to estimate the capacity (*34*).

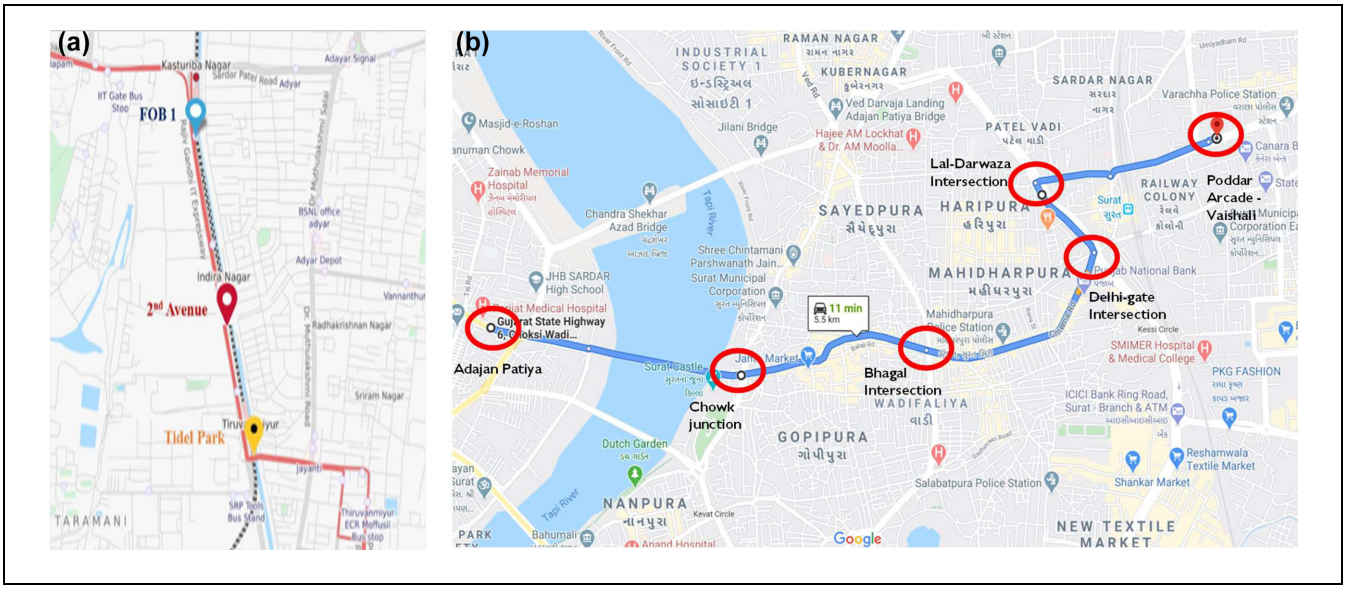

Figure 1. Snapshot of study locations: (*a*) urban arterial in Chennai and (*b*) urban network in central business district of Surat city.
Note: FOB = Foot Over Bridge.

Performance Measure of Model

The above nonlinear optimization problem was solved using the generalized reduced gradient method. The performance of the model is measured as mean absolute percentage error (MAPE), root mean square error (RMSE), and mean percentage error (MPE). The following formulas are used to determine the MAPE, RMSE, and MPE.

$$\text{MAPE}(\%) = \frac{100}{n}\sum_{i=1}^{n}\left|\frac{(x_0 - x_p)}{x_0}\right|, \tag{20}$$

$$\text{RMSE}(\text{s}) = \sqrt{\sum_{i=1}^{n}\frac{(x_0 - x_p)^2}{n}}, \tag{21}$$

$$\text{MPE}(\%) = \frac{100}{n}\sum_{i=1}^{n}\frac{(x_0 - x_p)\times 100}{x_0} \tag{22}$$

where x_o = observed value, x_p = predicted value, and n = number of observations.

Data

Empirical Data

The traffic data were collected using Wi-Fi sensors for an urban arterial corridor along the Rajiv Gandhi IT expressway in Chennai (the southern part of India). The selected test bed section is a six-lane, divided (with access lane on either side), interrupted urban arterial corridor. It has two signalized intersections (one at 2nd Avenue and another at Tidel Park) along its length of 1.70 km, as shown in Figure 1*a*. The intersection at 2nd Avenue is a three-legged police-controlled, undersaturated signalized intersection. The average red time is about 60 s with a cycle time of 120 s. Tidel Park is a four-legged fixed-time signalized intersection. The average red time for the Tidel intersection is 244 s, with an average cycle time of 396 s. The intersection operates under oversaturated conditions during peak hours, with an average queue length of over 200 m.

Wi-Fi sensors were placed along the median at the midblock and the signalized intersections (*35*, *36*). However, it was deemed appropriate to position the sensor along the downstream end of the signalized intersection. The sole motive for placing the sensor at the downstream end was to incorporate the effect of the signalized intersection on travel times. Further, the sensors were mounted on an electrical pole (for providing a continuous power supply) at the height of 2.5 ft at the signalized intersection. At the midblock section, sensors were placed on Foot Over Bridge (FOB) (16 ft height). An antenna gain of 5 dBi (average coverage radius = 70 m) was polarized vertically to maximize data collection efficiency (*37*). The data were collected for 7 weeks, from May 18, 2018 to July 4, 2018. Videography surveys were also conducted during peak hours to comprehend the performance of the Wi-Fi sensors.

Data Processing

The travel time of an individual media access control (MAC) address from Wi-Fi sensor x upstream of sensor y is computed by matching the unique address of the

device carried by the vehicle and the corresponding time stamps. The present study considered the first to last (FILO) component for deriving travel time (*38*). Note that since the sensors were kept at three locations, only those MAC addresses whose trajectory was detected at all three locations were considered. This was done to retain the characteristics of the trip by extracting information using the intermediate sensor (the sensor placed at 2nd Avenue). The data processing procedure suggested by Singh et al. (*38*) was adopted in this study. For the empirical data, the traffic flow descriptors, such as travel time, traffic flow, traffic density, and TTU, were computed at a 15 min data aggregation interval. For 7 weeks, a total of 3265 data points were obtained. The travel time values derived using Wi-Fi detections were compared with the travel time collected using Google API. The error in travel time varied from 6% to 11%. The density plot of residuals was also observed to follow a normal distribution.

Data for Simulation

A network in the central business district of Surat city, India, was selected. The study network is about 6.0 km in length and has varying roadway geometry (four-lane divided, four-lane undivided, and six-lane divided roadway configuration) and intersection control (signalized, unsignalized, roundabouts); it is shown in Figure 1*b*. The subject study network consists of six major intersections, of which three are signalized, and the remaining three are unsignalized or uncontrolled intersections. The traffic video data for 21 h (from 3 a.m. to midnight) for all the signalized intersections and major access points were collected simultaneously under normal weather conditions. The classified volume count was extracted manually from the recorded videos because of the absence of a reliable automatic traffic data extractor. Therefore, 50 h of manual effort were put into extracting the time-series traffic volume data for one intersection. Travel time data were collected using a Performance Box (Racelogic). Performance Box is an instrument that has a GPS unit that records the latitude, longitude, and velocity at every 0.1 s. The recorded data are then used to obtain travel time (for links and network) and delay (for each intersection approach). Since traffic is heterogeneous in India, travel time data for 15 runs for each vehicle type during various conditions are collected. These data are used as input into simulation modeling.

Simulation Modeling

In India, the absence of proper instrumentation for effective data collection makes it difficult to simultaneously collect traffic data (traffic volumes and travel time) over space and time. Therefore, in the present study, the applicability of the proposed MBPR is also justified for an urban network using microsimulation. The present study simulated the urban network in VISSIM 9.0 (*39*). The framework adopted for calibration and validation of the traffic simulation model is illustrated in Figure 2.

Model Calibration

The network in the simulation model was developed by first modeling intersections using links and connectors. Using the road geometry detail extracted using Google Earth, the links between intersections were modeled. The static dimensions (length and width) of different vehicle types were adopted as reported in the literature (*40*) and given inputs to the simulation model to replicate the Indian traffic conditions. The stochastic variables such as classified volume count, routing decisions, and proportions of turning traffic were inputted into the simulation model at every 5 min aggregation interval. VISSIM includes the distribution of vehicle acceleration and deceleration performances as a function of the speed profile. Specific distributions were assigned to specific modes. The travel time data collected using the Performance Box were used to define different vehicle types' desired speed distribution profiles. The intersection timing scheme for signalized intersections, conflict areas, and priority rules for unsignalized intersections were also provided as inputs to the simulation model. In India, traffic conditions are heterogeneous and show weak lane discipline. Therefore, the driving behavior parameters for three types of behaviors, namely vehicle following, lane change, and lateral movement, were calibrated. The present study used a genetic algorithm to calibrate the driving behavior parameters. The objective function was formulated as

$$\min Z = \sum [\text{observed response} - \text{modelled response}]^2. \quad (23)$$

Network travel time was considered a measure of effectiveness (MOE) to calibrate the driving behavior parameters. A MATLAB script was developed to operate the VISSIM through the COM interface. The optimization runs were carried out repetitively with a change in population size and number of stall generations. An initialization period or warm-up time of 30 min was adopted before extracting outputs. This was done to ensure that the system reached equilibrium (*41*). The driving behavior parameters were calibrated for each vehicle type, and the results are summarized in Tables 1 to 3. In the case of the vehicle-following behavior, the Wiedemann-74 model was calibrated. The selection of the Wiedemann-74 model was appraised based on past literature (*42*, *43*).

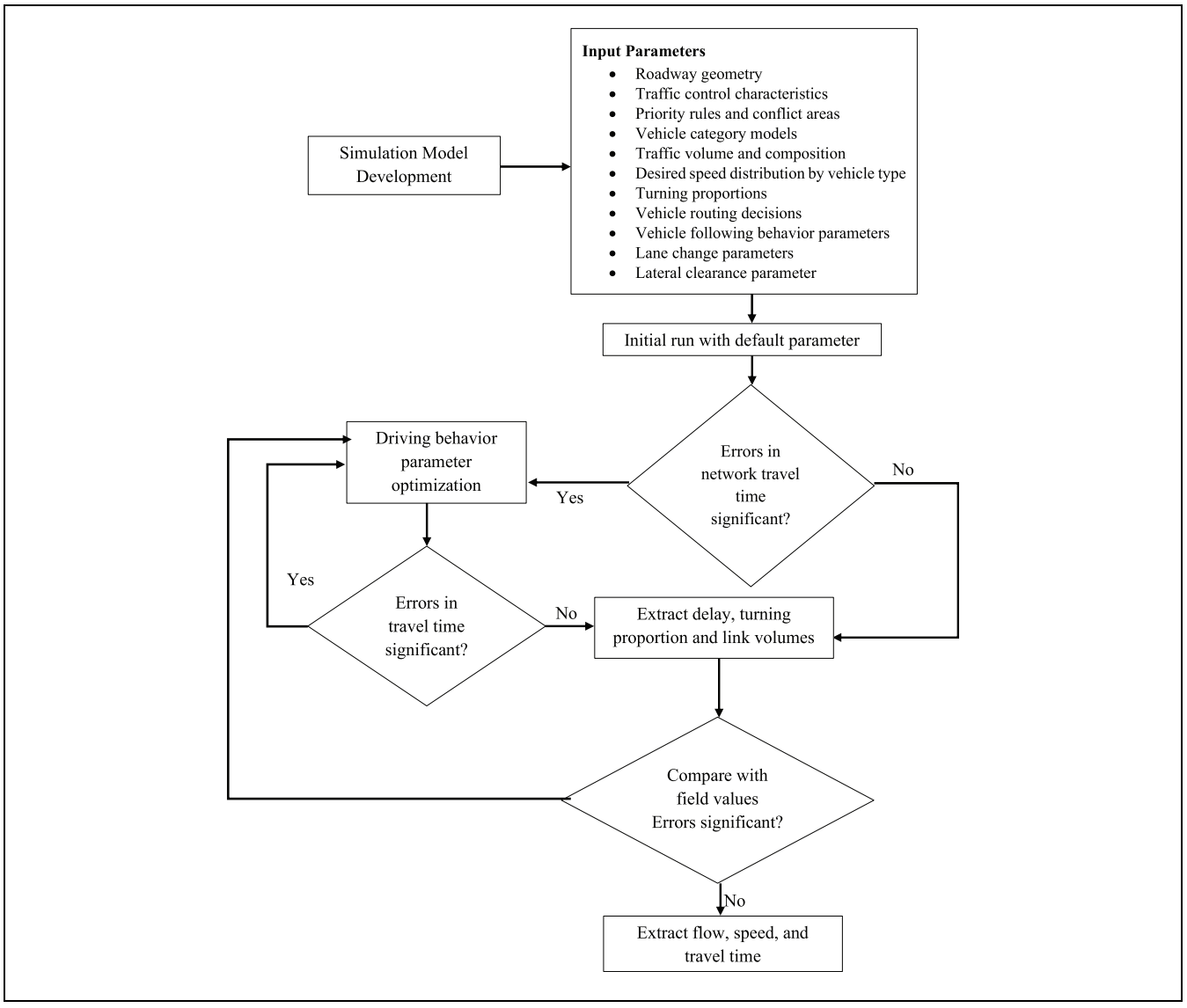

Figure 2. Methodology for calibration and validation of microsimulation model.

The optimized values of driving behavior parameters were in close approximation to those reported by Chepuri et al. (*42*) and Paul et al. (*43*). The developed simulation model was run using the 21 h collected field data. Corresponding travel time data for each link were collected using travel time counters to validate the simulation model. Figure 3 illustrates the cumulative distribution plot of field observed travel time and simulated travel time for the network on the same axes.

Figure 3 shows that the travel time obtained through simulation is close to those observed in the field. Consistent observations can be noted for different vehicle categories. MAPE values for different vehicle categories were computed. It was observed that MAPE values for different vehicle types are less than 8% which highlights the robust calibration of the simulation model (driving behavior parameters). Further, a two-sample K-S test at a 5% significance level was also performed. It was concluded that the K-S test statistic was lower than the critical value at a significance level of 0.05% for different vehicle categories. This highlights that the traffic simulation model is well-calibrated.

Model Validation

The well-calibrated model was also validated at three resolutions (a) link volumes, (b) turning proportions at intersections, and (c) delay at intersections. The

Table 1. Calibrated Wiedemann-74 Parameters for Different Vehicular Categories

Parameter	Vehicle category			
	M2W	M3W	Car/LCV	Bus/truck
Average standstill distance (m)	0.2	0.2	0.4	0.4
Additive part of safety distance	0.3	0.3	0.5	0.5
Multiplicative part of safety distance	0.5	0.5	0.7	0.75

Note: M2W = motorized two-wheelers; M3W = motorized three-wheelers; LCV = light commercial vehicles.

Table 2. Calibrated Lateral Clearance Values

Vehicle category	Lateral clearance share (m)	
	@ 0 km/h	@ 50 km/h
M2W	0.20	0.35
M3W	0.20	0.35
Car/LCV	0.20	0.5
Bus/Truck	0.40	0.7

Note: M2W = motorized two-wheelers; M3W = motorized three-wheelers; LCV = light commercial vehicles.

simulation model was validated for data corresponding to evening peak hours (5 to 8 p.m.), whereas the morning peak data (8 to 11 a.m.) and off-peak hours (periods other than morning and evening peak) were used for calibration of the simulation model.

Validation of Link Volumes. The link volumes for each link extracted using simulation were compared with those observed in the field, and errors in link volumes were estimated. Table 4 summarizes the error values observed in traffic volumes for each intersection of the study network.

From the table, it can be noted that the errors (MAPE and MPE) in link volumes are less than 20% for all the links considered in the study. This highlights that the calibrated simulation model can predict the link volumes and, thus, represent the field condition aptly.

Validation of Turning Proportion at Intersections. The turning proportions were extracted from the simulation model and were compared with the field observed turning proportions. A node boundary was created around each intersection to extract turning movements at the intersection. The comparison of field observed turning proportions and turning proportions extracted from the simulation model is shown in Figure 4 for two intersections as an example. Figure 4 shows that the turning proportions from the simulation model match those observed in the field. Consistent observations were noted for other intersections as well.

Validation of Delay at Intersections. Delay values for each intersection approach were computed using the Performance Box data. The results were compared with the delay values obtained using the simulation model, as shown in Figure 5. Here, delay comparison is shown for all approaches of one intersection.

Delays obtained using simulation are similar to those observed in the field. The statistical validation of this observation was done by performing a one-sample paired *t*-test at a 5% level of significance. The results revealed no significant difference between the delay extracted from the simulation model and the delay observed in the field. MAPE values were calculated and observed to be less than 10% for all the approaches. Consistent observations were noted for other intersections in the network. Overall, it can be concluded that the developed simulation model is well-calibrated and, thus, represents the field observed conditions reasonably well (error less than 15% for all resolutions of validation).

Table 3. Calibrated Lane Change Parameters

Parameters	Vehicle category							
	M2W		M3W		Car/LCV		Bus/truck	
	L	F	L	F	L	F	L	F
Maximum deceleration (m/s^2)	4.85	5.22	4.39	4.76	3.82	2.24	4.13	3.90
Negative 1 m/s^2 per distance	20	20	25	25	45	45	45	45
Accepted deceleration (m/s^2)	1.00	1.00	1.00	1.00	1.00	1.00	1.00	1.00
Minimum headway (front/rear) (m)	0.40		0.40		0.50		0.40	
Safety distance reduction factor	0.50		0.50		0.50		0.50	
Maximum deceleration for co-operative braking (m/s^2)	4.58		3.35		1.12		2.41	

Note: M2W = motorized two-wheelers; M3W = motorized three-wheelers; LCV = light commercial vehicle; L = Leader; F = Follower.

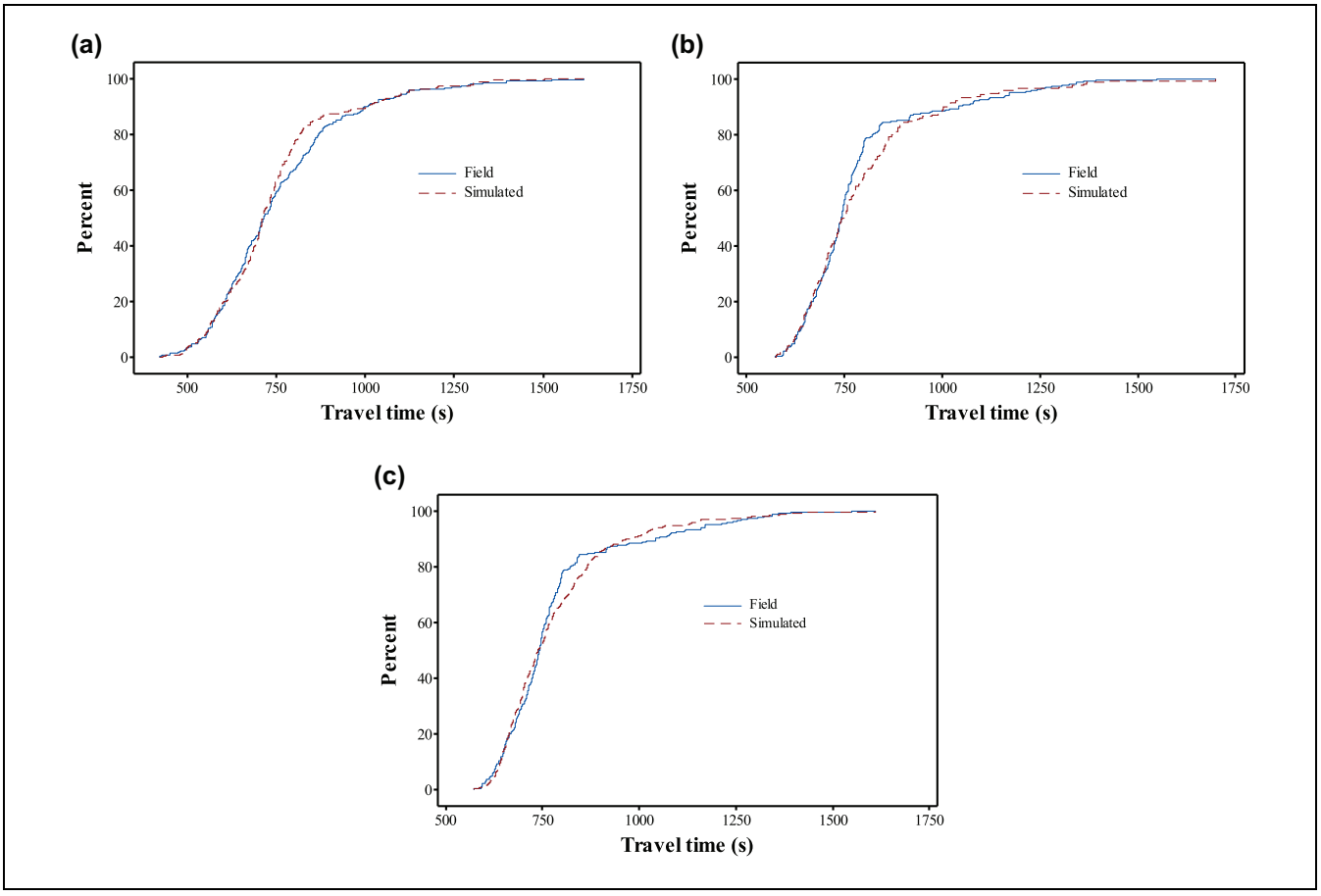

Figure 3. Cumulative travel time distribution profiles for: (*a*) cars, (*b*) motorized two-wheelers, and (*c*) motorized three-wheelers.

Table 4. Validation of Entry–Exit Volumes

Link direction	MPE (%)	MAPE (%)	Link direction	Error (%)	MAPE (%)
A–C	13.77	14.77	C–A	9.653	12.45
C–B	14.01	15.98	B–C	15.96	15.87
B–DG	0.261	6.26	DG–B	14.43	17.77
DG–LD	6.287	9.65	LD–DG	8.002	10.93
LD–PA	11.76	15.76	PA–LD	5.834	9.53

Note: MPE = mean percentage error; MAPE = mean absolute percentage error; A = Adajan Patiya; C = Chowk junction; B = Bhagal intersection; DG = Delhi-gate intersection; LD = Lal-Darwaza intersection; PA = Podder Arcade Vaishali.

Fundamental and Macroscopic Fundamental Diagram Estimation

Fundamental Diagram Estimation Using Wi-Fi Detections

In a real-world application, the traffic parameters like traffic flow and density can be computed if the detailed trajectories of all the vehicles are provided. However, if these data are only provided for a subset of vehicles (like Wi-Fi probes), Edie's generalized definition to estimate the traffic parameters cannot be applied directly. Nagle and Gayah (*44*) and Du et al. (*45*) adopted the penetration rate as an approximation to estimate flow and density, assuming that the penetration rate is known. Nagle and Gayah (*44*) and Shim et al. (*46*) adopted a uniform penetration rate across the network to compute flow and density. Considering that the penetration rates are likely to be non-uniform across space and time (*45*, *47*), a relation between sensor-recorded volume and penetration rate was developed in the present study. This relation

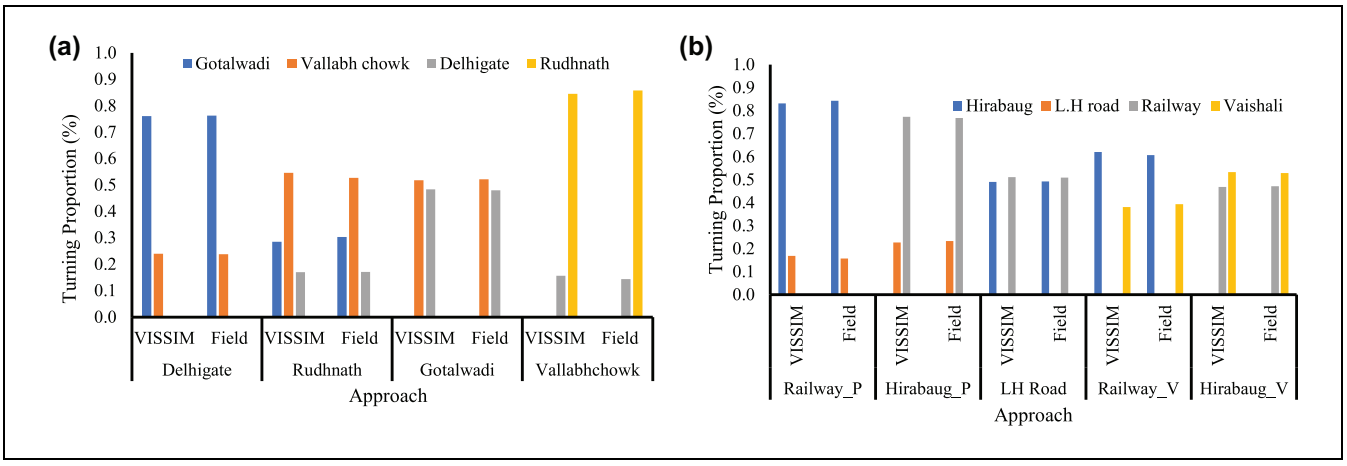

Figure 4. Comparison of turning proportions: (*a*) Lal-Darwaza intersection and (*b*) Poddar Arcade intersection.

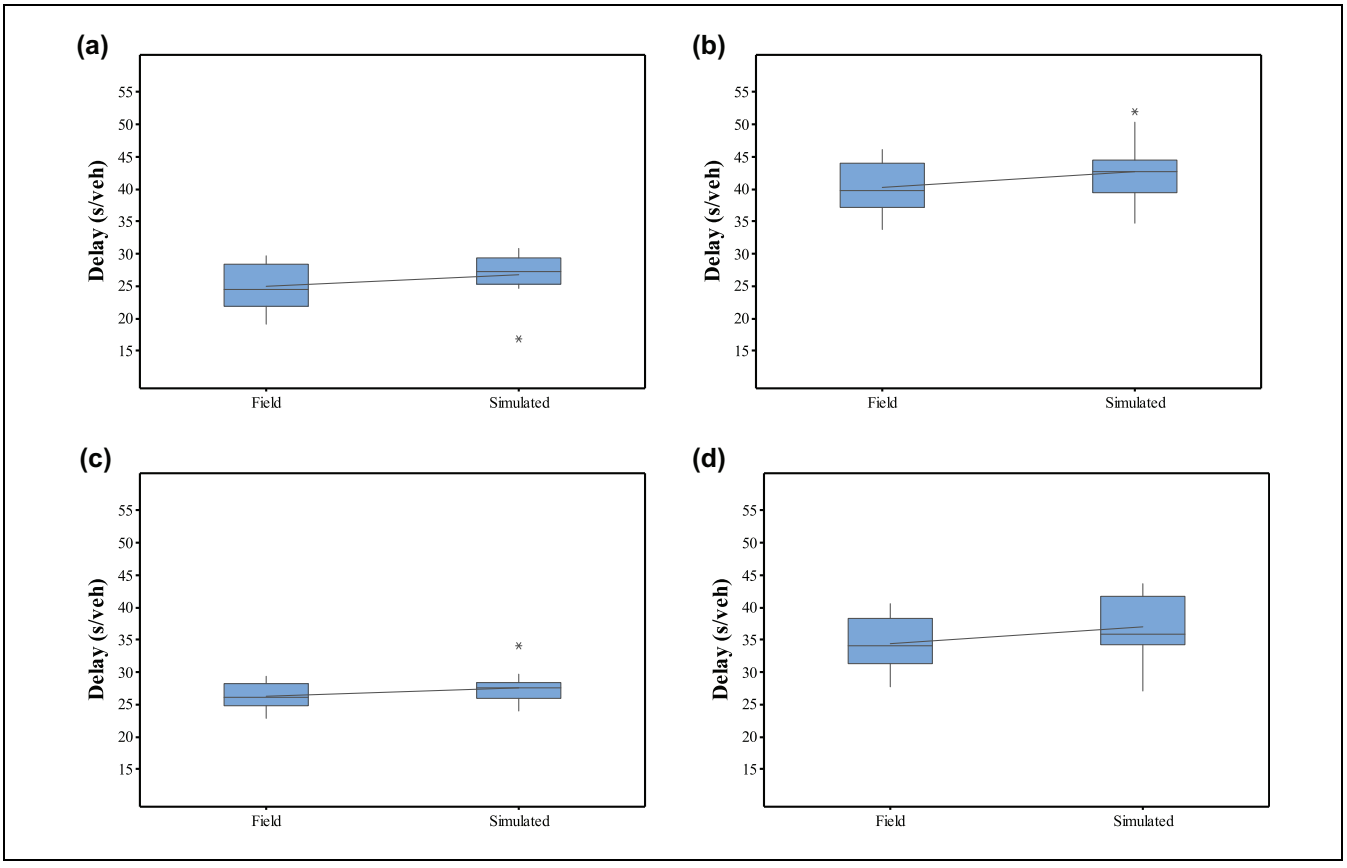

Figure 5. Comparison of field observed delay and delay obtained through simulation model. Legends are as follows: (*a*) Hirabaug to Railway Station, (*b*) LH Road to Hirabaug, (*c*) Railway Station To Hirabaug, and (*d*) Railway Station to LH Road.
Note: s/veh = seconds per vehicle.

was used to derive penetration rates, traffic flow, and density.

Three main variables to visualize the traffic stream (traffic flow, density, and speed) were computed using the data derived from the Wi-Fi sensor and the video data. A directional factor (ADD) was introduced since Wi-Fi sensors could capture traffic volumes on either side. Further, since multiple patches from a single vehicle (evidence of vehicle occupancy) can occur, an average vehicle occupancy (AVO) factor was introduced to estimate flow and density. The methodology suggested by Gore et al. (*48*) was adopted to derive vehicle occupancy

for the present section. The traffic stream variables were computed for a 15 min aggregation interval. The traffic stream variables are given by

$$Q = \frac{\mathrm{QS}}{\rho \mathrm{AVOADD}}, \tag{24}$$

$$K = \frac{\sum_{i=1}^{n} \left(\frac{t_i}{l_r}\right)}{mT\mathrm{AVO}}, \tag{25}$$

$$V = \frac{l_r}{\frac{\sum_{i=1}^{n} t_i}{n}} \tag{26}$$

where

Q = traffic flow (in one direction);
QS = traffic flow recorded by the sensor;
ρ = penetration rate;
m = matching rate;
AVO = average vehicle occupancy (in the case of Wi-Fi or Bluetooth data) (AVO is 1.65 for the present case);
ADD = average directional distribution factor (60% for FOB to Tidel and 40% for Tidel to FOB from field data);
K = traffic density;
t_i = travel time by ith vehicle;
l_r = length of the route;
T = observation window (15 min for the present case);
n = number of vehicles recorded by the sensor; and
V = traffic speed.

The penetration rate is not considered in extrapolating traffic density. It was observed from the dataset that not all the vehicles identified at the inflow location matched at the other end. Therefore, only the vehicles matched at both ends were considered for extrapolating traffic density. It is important to note that the penetration rate derived using the penetration rate model varies over time based on the sensor-recorded traffic flow for the subject corridor. Further, the matching rate, which can also be expressed as a function of penetration rate, also varies over time. Therefore, dynamic values of both penetration rate and matching rate are considered in the present study. It should be noted that an error in traffic flow estimated using Equation 24 ranges from 100 vph to 350 vph. Similarly, an error in estimating traffic density ranged from 5% to 15%.

Macroscopic Fundamental Diagram Using Simulated Data

The calibrated simulation model was run using the 21 h field data. Traffic flow descriptors such as traffic flow, speed, and travel time extracted for each link, were used to compute network-wide traffic flow parameters. The density for each link was computed using the fundamental equation of traffic flow (*49*). The network-wide traffic flow parameters were computed using the following equations at every 5 min aggregation interval (*50*).

$$K = \frac{\sum_{x=1}^{5} (k_x \times l_x)}{\sum_{x=1}^{5} l_x} \tag{27}$$

$$V = \frac{\sum_{x=1}^{5} (v_x \times l_x)}{\sum_{x=1}^{5} l_x}, \tag{28}$$

$$Q = \frac{\sum_{x=1}^{5} (q_x \times l_x)}{\sum_{x=1}^{5} l_x} \tag{29}$$

where K, V, and Q are network-level macroscopic flow parameters; k, v, and q are macroscopic flow parameters for each link; l is the length of each link.

It is essential to mention that traffic flow variables like traffic flow, traffic density, travel time, speed, and TTU are computed at every 15 min aggregation interval for empirical data and every 5 min aggregation interval for the simulated dataset.

Results and Discussions

Fundamental Diagram: Empirical Data

Figure 6 represents the FD for the study corridor. Here, FD is plotted for individual days. The motive for plotting an FD for individual days was to understand the variation in speed and traffic flow across different days for a given traffic density value. This assists in comprehending whether the systems are in stable or unstable states. Here, the traffic density is not computed per lane because of non-lane-based traffic conditions in India. Under such traffic conditions, the vehicles do not follow lane discipline and can occupy any position on the roadway, and as a result, density or flow is not expressed as per lane.

From the figure, it can be inferred that a wide variation in stream speed and traffic flow exists for similar density values. Further, it is interesting to note that lower speeds correspond to lower densities for some days. Thus, higher congestion can be observed during low-density conditions as well. This could be attributed to traffic incidents, weather (heavy rains), or special events like holidays/festivals. Further, high proportions of turning movements during specific periods (*49*) and the effect of the cyclic nature of signalized intersections (*51*, *52*) could also lead to reduced speeds during low flow conditions. For the present case, the two signalized intersections (at 2nd Avenue and Tidel Park) are closely spaced (the distance between the two is less than 600 m) with different cycle lengths of 120 s and 396 s and a green-to-cycle time (g/C) ratio of 0.25 and 0.50, respectively. The average queue length between the two intersections also varies significantly. This variation in g/C ratio, signal

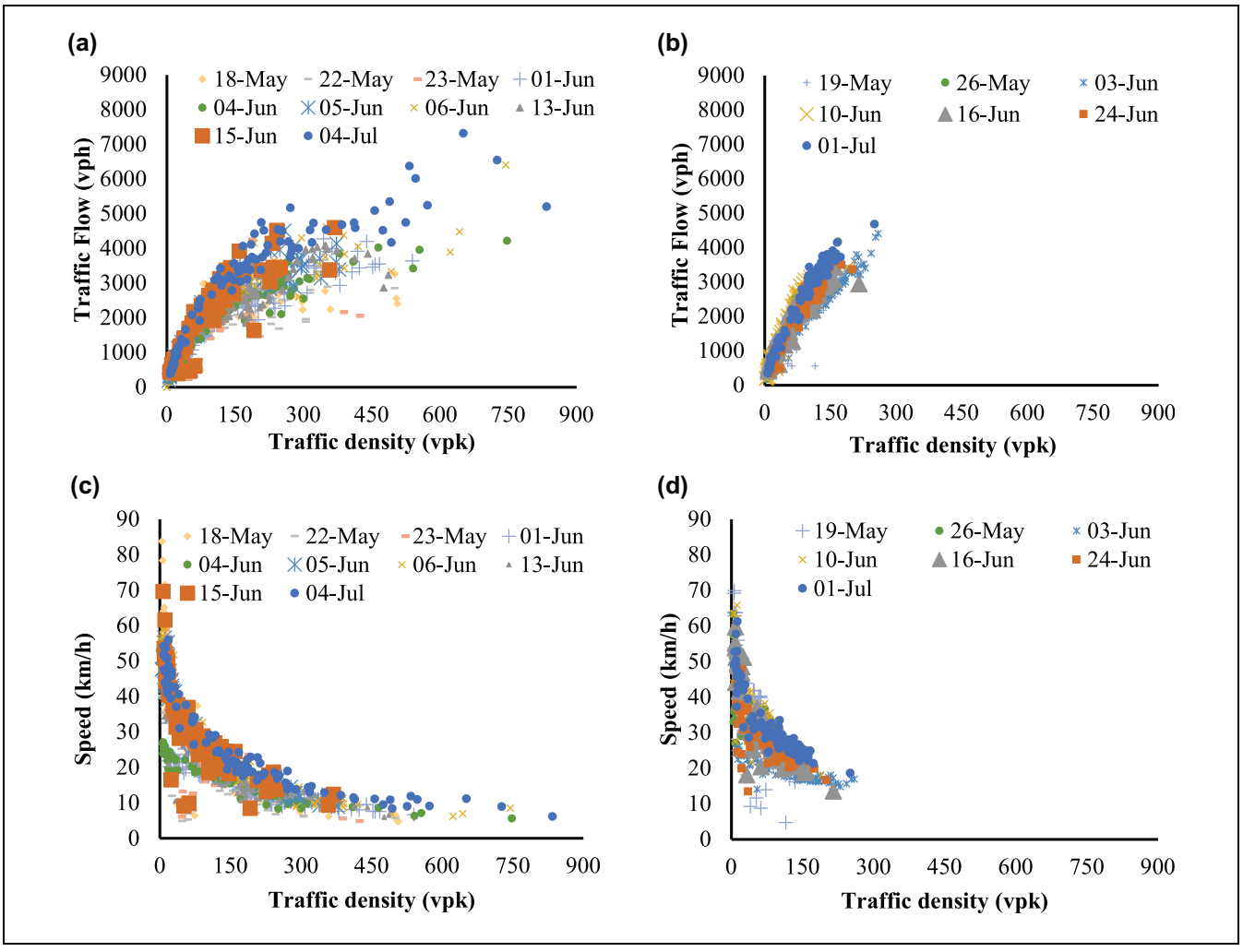

Figure 6. Flow–density and speed–density relations for weekdays and weekends using empirical data: (*a*) *Q*–*K* relation (weekdays), (*b*) *Q*–*K* relation (weekends), (*c*) *V*–*K* relation (weekdays), and (*d*) *V*–*K* relation (weekends).
Note: vph = vehicles per hour; vpk = vehicles per kilometer; *Q* = traffic flow; *K* = traffic density; *V* = speed.

cycle length, and queue length results in large variations in the FD.

Macroscopic Fundamental Diagram: Simulated Data

Figure 7 illustrates the MFD developed for the urban network between Adajan Patiya (A) and Podder Arcade (PA) using simulated data. Here, the MFDs are plotted by the direction of travel—that is, a separate MFD is developed for (A–PA) movement and (PA–A) movement.

The MFD and speed–density relation varied when analyzed by direction of travel, attributed to varying roadway geometry, traffic control, and its characteristics. For example, the difference in g/C ratio and phasing scheme between north–south and south–north movement can induce a variation in MFD. Further, it can be noted that lower speeds are observed for low-density conditions. This could be attributed to the cyclic nature of intersections, variations in turning proportions, and roadway and traffic control characteristics. Ambühl et al. (*53*) reported three reasons for the variation in MFD: (1) traffic is dynamic in cities and is rarely in a steady state, (2) heterogeneity in the spatial distribution of vehicles, and (3) interaction of public transport operations with vehicle flows. In addition, the variation in MFD can be attributed to the variation in road functional classes and network topological factors (roadway geometry, traffic control type and its characteristics) (*54*).

From Figures 6 and 7, it can be concluded that the changes in travel time under similar traffic flow conditions may vary significantly with different circumstances (*23*) and indicate that the relation between traffic flow variables is stochastic.

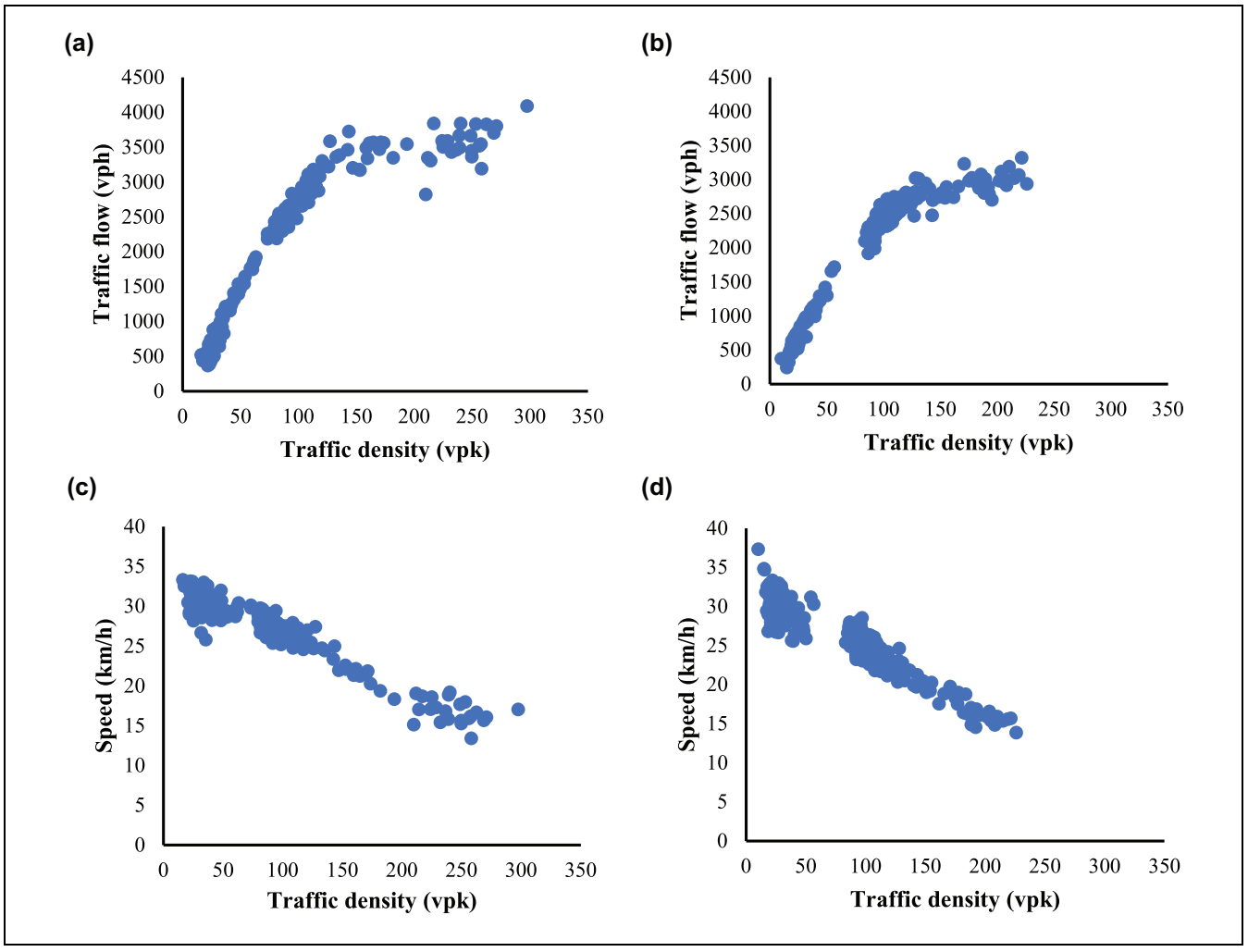

Figure 7. Flow–density and speed–density relations for the network using simulated data: (*a*) *Q*–*K* relation (A–PA), (*b*) *Q*–*K* relation (PA–A), (*c*) *V*–*K* relation (A–PA), and (*d*) *V*–*K* relation (PA–A).
Note: vph = vehicles per hour; vpk = vehicles per kilometer; *Q* = traffic flow; *K* = traffic density; *V* = speed; A = Adajan Patiya; PA = Podder Arcade.

Effect of TTU

To investigate the effect of TTU, a scatter of TTU against traffic density is plotted for both empirical (Figure 8, *a* and *b*) and simulated (Figure 8, *c* and *d*) datasets, as shown in Figure 8.

Figure 8 shows that TTU increases with an increase in density. The observations are consistent for both empirical and simulated datasets. Vehicle-to-vehicle interaction influences travel time distribution at higher densities; therefore, higher TTU at higher density can be attributed to unstable traffic flow. Further, it is interesting to note that, for low-density conditions, higher values of TTU can be noted, highlighting that the travel time under low-density conditions is uncertain. Higher TTU for lower densities indicates that uncertain travel times are caused by supply-side influencing factors, that is, the cyclic nature of signalized intersections, varying roadway, traffic control characteristics, and variation in traffic composition. Lower speed values for lower density values could be attributed to higher values of TTU. Therefore, it can be concluded that TTU significantly affects travel time, especially in free-flow conditions. The observation is consistent with Ngoduy (*30*) and Li et al. (*31*).

Calibration Results

As discussed in the "Methodology" section, two parameters, free-flow travel time (t_f) and capacity (C_a), derived using empirical and simulated datasets, were fixed for calibrating the BPR and the MBPR function. This was done to derive a more robust fit (*32*). The free-flow travel time and capacity values are estimated

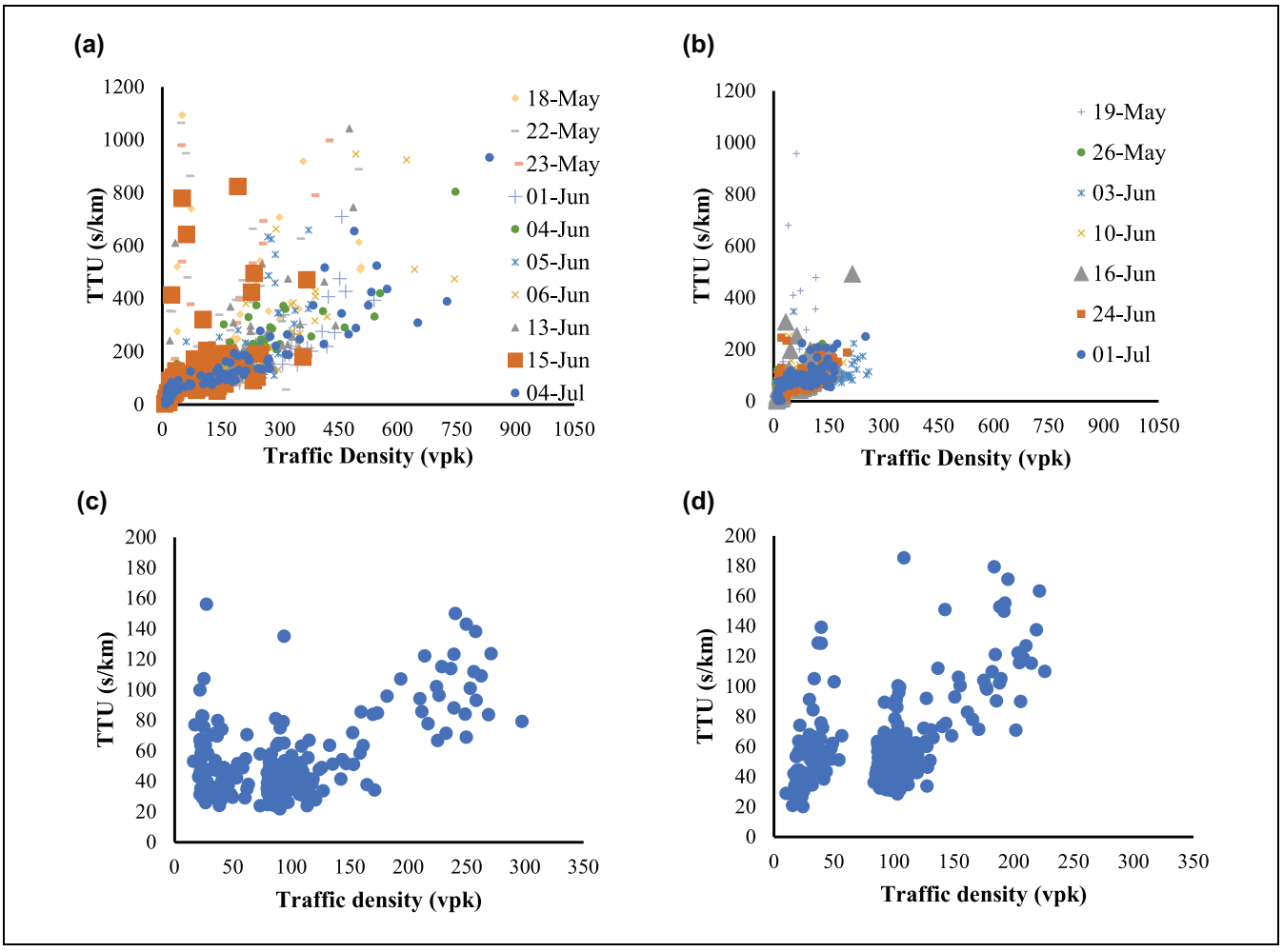

Figure 8. Variation in TTU with traffic density: (*a*) TTU–*k* relation (weekdays empirical data), (*b*) TTU–*k* relation (weekends empirical data), (*c*) TTU–*k* relation (A–PA simulated data), and (*d*) TTU–*k* relation (PA–A simulated data).
Note: TTU = travel time uncertainty; *k* = traffic density; A = Adajan Patiya; PA = Podder Arcade.

as discussed in the "Methodology" section, and the estimated values of free-flow travel time and capacity for empirical and simulated datasets are explained next.

Empirical Dataset. A free-flow travel time of 102 s was obtained for empirical data, corresponding to a free-flow speed of 60 km/h for a route length of 1.70 km. The obtained free-flow speed for the empirical dataset is consistent with that reported by Thankappan and Vanajakshi (*55*) for the same study section. The capacity value 5550 vph or 1850 vphpl (vehicles per hour per lane) for a three-lane urban arterial corridor was obtained using the generalized polynomial function. The capacity value of 5550 vph is also in line with Das and Rama Chilukuri (*2*) reported for the same study corridor.

Simulated Dataset. Free-flow travel time of 648.59 s for A–PA (network length of 5.69 km) and 665.26 s for PA–A (network length of 5.93 km) was obtained. Capacities of 4715 vph and 4365 vph were obtained for the network in a north–south direction (A–PA) and south–north (PA–A), respectively. Similarly, free-flow travel time and capacity were evaluated for each of the links of the network.

Calibration Results: Empirical Data

The BPR and MBPR function was calibrated for 17 days, that is, from May 18 to July 4, 2018, where 24 h time-series data were available. The optimization program was repeated until the convergence was not obtained. Sample calibration results for 2 days are shown in Figure 9 as an example. Consistent results were noted for other days as well.

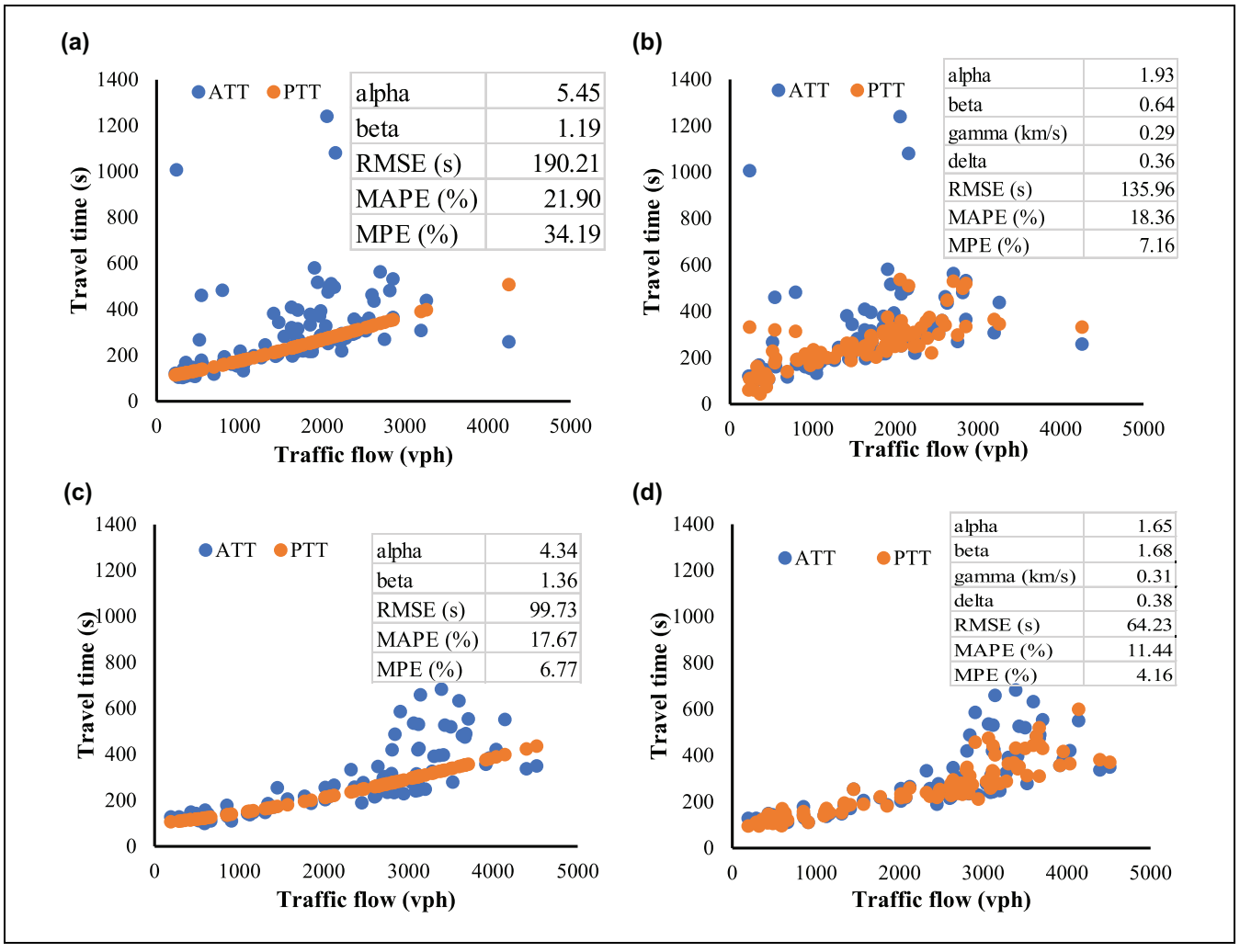

Figure 9. Calibration result of BPR and MBPR function for empirical dataset: (*a*) BPR, (*b*) MBPR, (*c*) BPR, and (*d*) MBPR.
Note: BPR = Bureau of Public Roads function; MBPR = modified BPR; ATT = actual travel time; PTT = predicted travel time; RMSE = root mean square error; MAPE = mean absolute percentage error; MPE = mean percentage error; vph = vehicles per hour.

Calibration Results: Simulation Data

The BPR and MBPR function was calibrated separately for each link, and the network in the north–south and south–northbound direction. The optimization program was repeated until the convergence was not obtained. The results are shown in Figure 10 for the network only. Consistent results were also obtained for links considered in the network.

Figures 9 and 10 show that the MBPR function fits the data (both empirical and simulated) well compared with the BPR function. This is visible from the reduction in the value of different performance measures like MAPE, MPE, and RMSE. Further, the MBPR function can predict multiple values of travel time corresponding to a specific value of traffic flow based on the values of TTU. Therefore, the MBPR function can better characterize and address the uncertainty or heterogeneity in travel time and traffic flow relation than can the existing BPR function.

Effectiveness of MBPR Function

The BPR function has known limitations that (a) it does not represent the oversaturated conditions (volume to capacity ratio greater than one) effectively, and (b) it ignores the time-dependent relation between traffic volume and delay. In the present study, the effectiveness of the MBPR function is justified by (a) comparing travel time and its variability in oversaturated conditions and (b) exploring the time-dependent relation between traffic volume and delay.

Performance in Oversaturated Conditions. For empirical and simulated datasets, traffic volume higher than the

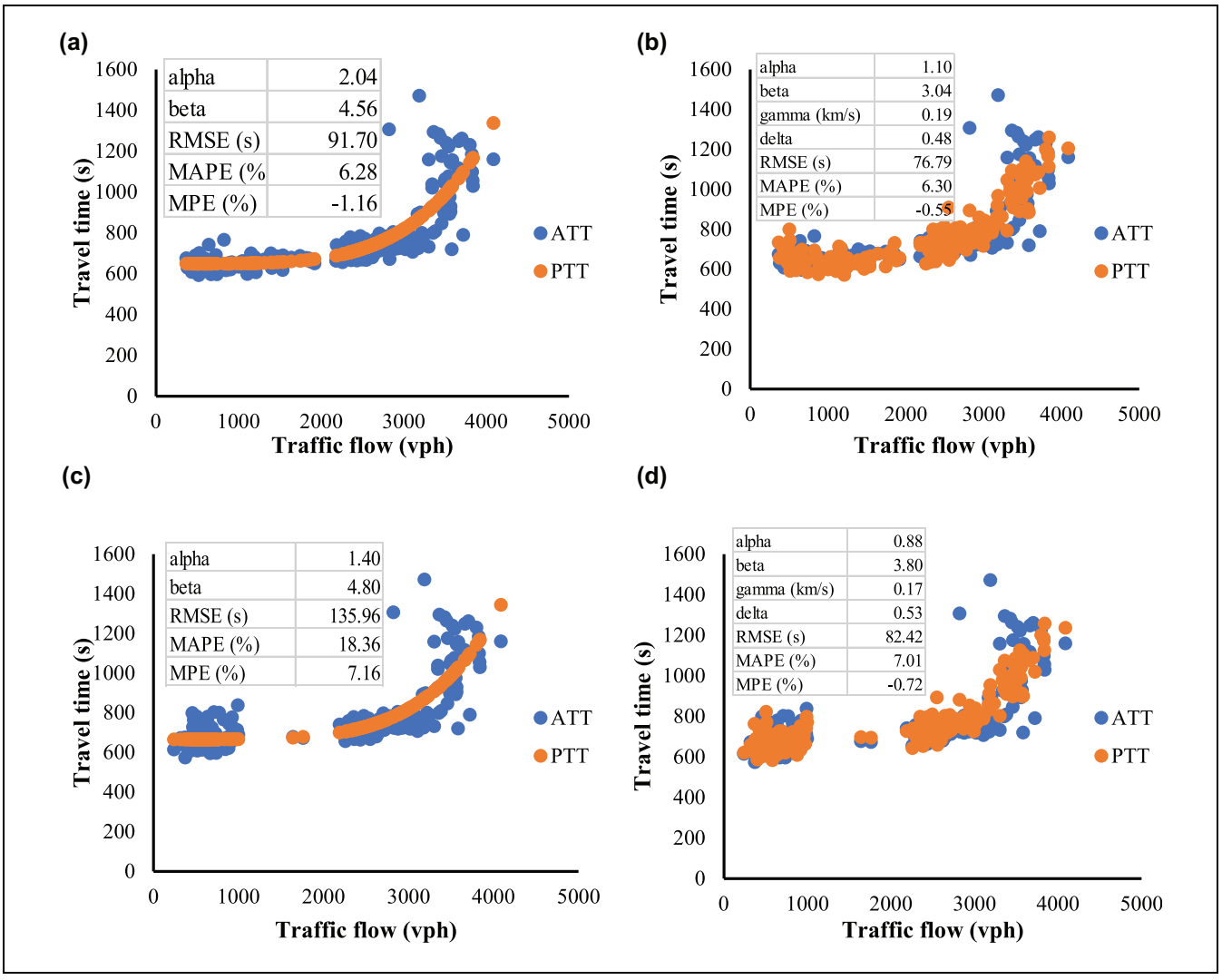

Figure 10. Calibration result of BPR and MBPR function for the simulated dataset: (*a*) BPR (A–PA), (*b*) MBPR (A–PA), (*c*) BPR (PA–A), and (*d*) MBPR (PA–A).

Note: BPR = Bureau of Public Roads function; MBPR = modified BPR; A = Adajan Patiya; PA = Podder Arcade; RMSE = root mean square error; MAPE = mean absolute percentage error; MPE = mean percentage error; ATT = actual travel time; PTT = predicted travel time; vph = vehicles per hour.

capacity was observed. Therefore, for the oversaturated conditions ($V/C > 1$), the observed travel time and travel time computed using BPR and MBPR were compared using cumulative percentile plots, as shown in Figure 11. It is essential to mention that oversaturated conditions were observed for a few links for the simulated dataset. The result related to one link is shown in Figure 11*b* as an example. However, for the entire network, oversaturated conditions were not observed.

Figure 11 shows that the observed travel time and the travel time predicted using MBPR are in close approximation, unlike those predicted using the BPR function. This implies that the MBPR function could also capture the variability of travel times under oversaturated conditions better than the BPR function. The statistical validation of this observation was done by performing a one-way ANOVA (analysis of variance) between the observed travel time and the travel time predicted using the MBPR function. For the MBPR function, the results revealed no significant difference between the observed and predicted travel time. A significant difference between the observed and predicted travel times was noted for the BPR function. Therefore, it can be concluded that the MBPR function can represent the oversaturated conditions better than the BPR function.

Time-Dependent Relation between Traffic Volume and Delay. Another drawback of the static volume–delay function is that it cannot capture the time-dependent relation between volume and delay. On the other hand,

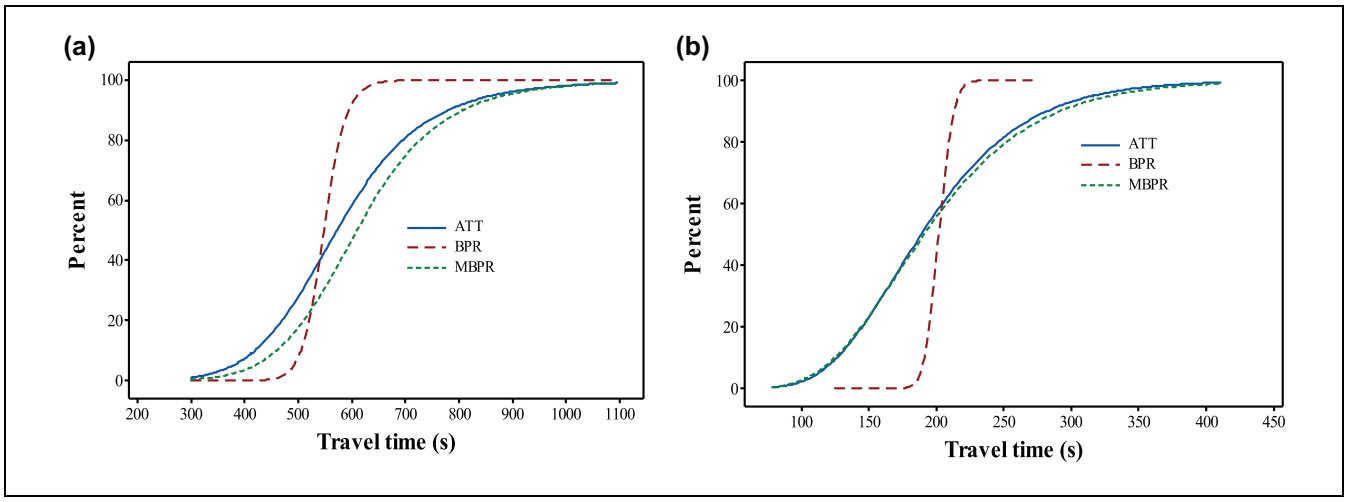

Figure 11. Comparison of BPR and MBPR under oversaturated conditions for: (*a*) empirical data and (*b*) simulated data.
Note: BPR = Bureau of Public Roads function; MBPR = modified BPR; ATT = actual travel time.

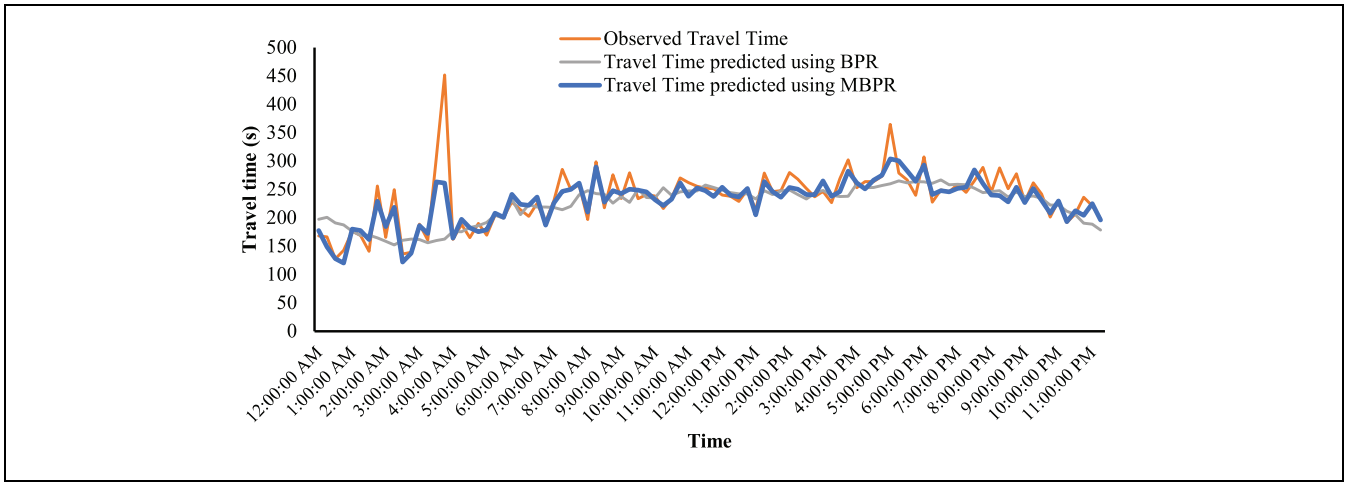

Figure 12. Temporal comparison between the observed and predicted travel time using BPR and MBPR function.
Note: BPR = Bureau of Public Roads function; MBPR = modified BPR.

MBPR would capture the time-dependent relation between volume and delay. This can be attributed to the inclusion of TTU in the formulation. The TTU would vary based on demand- and supply-side factors. For instance, if the traffic flow transits from an undersaturated to an oversaturated condition, then the magnitude of TTU for both the conditions will be correlated. The temporal comparison between the observed and predicted travel time using the BPR and the MBPR function is shown in Figure 12.

From Figure 12, it can be concluded that the MBPR function also accounts for the time-dependent relation between traffic volume and delay. The normalized RMSE (RMSN) was evaluated for travel times predicted using the BPR and the MBPR. It was observed that RMSN was 0.20 for the BPR function, whereas the same for the MBPR function was 0.10. The reduction in RMSN for MBPR highlights that the MBPR function has better prediction capabilities than the BPR function Further, Figure 12 highlights specific trends in the evolution of traffic flow over a given day. A spike can be observed during peak hours 5 p.m. This peak can be attributed to an increase in traffic volume and changes in the cycle time at signalized intersections. The intersection at 2nd Avenue is police controlled. This means that the cycle time and the green time varies as per the perception of the traffic police. This is quite similar to adaptive signal control. The continuous changes in green time and the cycle time during peak periods cause a change in supply. Therefore, changes in demand and supply cause a

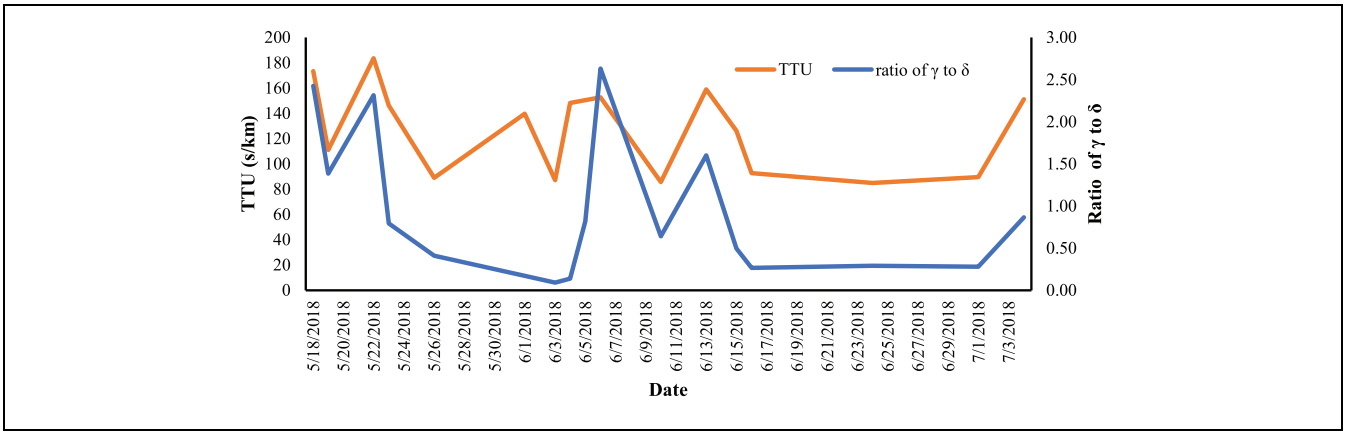

Figure 13. Analysis of inter-day heterogeneity.
Note: TTU = travel time uncertainty.

significant change in the magnitude of TTU, resulting in significant travel times. This phenomenon is captured if uncertainties are incorporated. However, this spike is not captured by the deterministic BPR. Therefore, the uncertainties or TTU in the present case capture the variation in travel time arising from changes in capacity (or supply) and demand. The spike in travel time at 4 a.m. could be a result of factors like heavy rains and lane closure and needs further detailed investigation, thus forming the future scope of the study.

One can argue that adding new variables to an equation would improve the model's performance. It is important to note that the added variable (TTU) in the present case captures the uncertainties in traffic flow, and because of this, varying travel time values for a given traffic flow condition are predicted. The uncertainties in traffic flow are attributable to two broad reasons: (a) demand or traffic volume and (b) supply (change in capacity resulting from traffic control, roadway geometry, and weather conditions). If the evolution of traffic flow is examined, it can be observed that the traffic flow constantly transits from one traffic state to another (refer to Figure 12, for example). This variation in traffic states results in varying TTU and travel time values. The variation in TTU between different traffic states and over periods is correlated, highlighting that TTU inherently entails the time-dependent nature of traffic flow. Because of this property of TTU, the MBPR function proposed in the present study (a) explains the stochastic nature of traffic flow, (b) represents the oversaturated conditions without the need for modified or oversaturated demand, and (c) explains the time-dependent relation between traffic flow and travel time. Therefore, incorporating TTU adds physical meaning to the BPR function.

Overall, it can be concluded that the MBPR function overcomes the disadvantages or limitations of the traditional BPR function. It is also important to note that the variables used in the MBPR function are easy to measure in the field using loop detectors, Wi-Fi/Bluetooth sensors, RFID (radio-frequency identification) sensors, and probe vehicle data.

Interpretations of γ and δ

In the "Methodology" section, the physical interpretations of γ and δ in respect of inter-day heterogeneity, infrastructure potential, and heterogeneity in the traffic flow distribution were discussed. Since the interpretations are related to inter-day heterogeneity, infrastructure potential, and traffic flow stability, they thus have significant practical applicability in traffic flow theory. In this subsection, these three interpretations are discussed in detail.

Inter-Day Heterogeneity. γ and δ are representative of the value of TTU. A higher value of γ and δ would indicate a higher value of TTU. It is expected that TTU would vary among links, and for a given link, TTU would vary between days. Therefore, variation in γ and δ can potentially explain the inter-day heterogeneity and variability in travel times. To support this observation, a line plot between TTU and the ratio of γ to δ is plotted for empirical data over different days, as shown in Figure 13. Here, the ratio of γ to δ is taken to consider the combined effect of γ and δ.

Figure 13 shows that both TTU and the ratio of γ to δ vary over different days. A higher ratio of γ to δ can be noted for the days with higher TTU values indicating a positive correlation between the TTU and the ratio of γ to δ. Therefore, the ratio of γ to δ can potentially represent the inter-day heterogeneity in travel times. The higher the value of the ratio of γ to δ, the more is the inter-day heterogeneity in traffic flow. Similarly, the

ratio of γ to δ can be compared between links of the network to conclude on heterogeneity in travel times and its uncertainty.

Infrastructure Potential. The second interpretation, as discussed in the "Methodology" section, suggests that for similar values of Q, TTU, α, and β, higher values of γ and δ would yield higher travel time than would lower values of γ and δ. To support this interpretation, two sets of γ and δ (0.32, 0.37; 0.49, 0.21) are considered. α and β values are fixed as 1.09 and 1.40, respectively. Figure 14 illustrates the variation in travel time for similar values of Q, TTU, α, and β for varying values of γ and δ.

From Figure 14, it is evident that for a similar α and β, Q, and TTU values, γ and δ have a significant effect on the values of travel time. For instance, if the ratio of γ and δ is higher (blue points), then for similar values of Q, TTU, α, and β, higher travel time values are observed compared with travel time values where the ratio of γ and δ is lower (orange points). This highlights that for a similar V/C ratio, days with a higher value of γ and δ, would indicate higher congestion in respect of travel times. Therefore, the infrastructure is not used efficiently. Thus, the values of γ and δ can represent the infrastructure potential.

Heterogeneous Distribution of Traffic Flow. The third interpretation relates the value of γ and δ to heterogeneity in the distribution of traffic flow. It is argued that if the ratio of γ to δ is higher, then the distribution of traffic flow over a given value of density is heterogeneous. The heterogeneous distribution of traffic flow over a given density value is estimated by analyzing the size of the hysteresis in MFD. Saberi and Mahmassani (*56*) reported that the size of the hysteresis could be quantified by its width and height and the area covered by the loop. A sample hysteresis plot is shown in Figure 15.

The size of the hysteresis can be expressed as an ordered pair of its width and height:

$$S_H = (\Delta k, \Delta Q). \tag{30}$$

The area of the hysteresis can be computed as

$$A_H = (\Delta k \times \Delta Q). \tag{31}$$

The area of hysteresis was computed for different links and networks. The area of hysteresis was normalized using capacity and critical density. The higher the value of the area of hysteresis, the more heterogeneous is the distribution of traffic flow. The normalized area of hysteresis was then correlated with the ratio of γ to δ, as shown in Figure 16.

From Figure 16, a positive correlation between the normalized area of hysteresis and the ratio of γ to δ is evident. It can be inferred that the higher the ratio of γ to δ, the larger the area of hysteresis. Thus, traffic flow is heterogeneously distributed over density, indicating instabilities in traffic flow. Therefore, the values of γ and δ can explain the heterogeneous distribution of traffic flow and thus can help comprehend the stability in traffic flow.

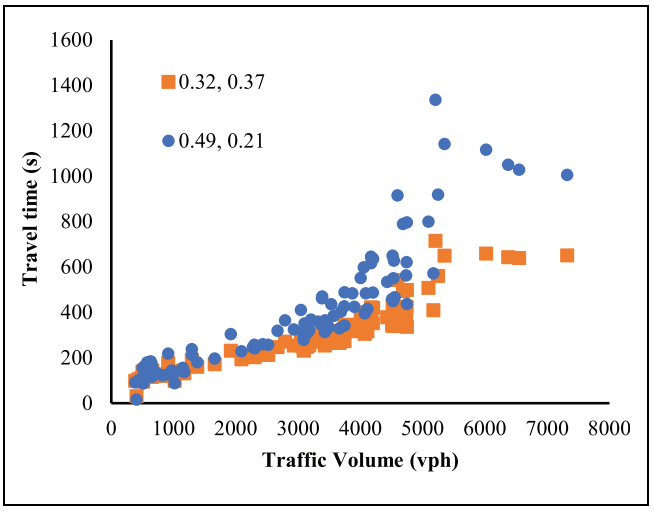

Figure 14. Variation in travel time values with changes in γ and δ values for similar values of α and β, traffic volume, and TTU.
Note: TTU = travel time uncertainty; vph = vehicles per hour. Orange points: γ = 0.32 and δ = 0.37; blue points: γ = 0.49 and δ = 0.21.

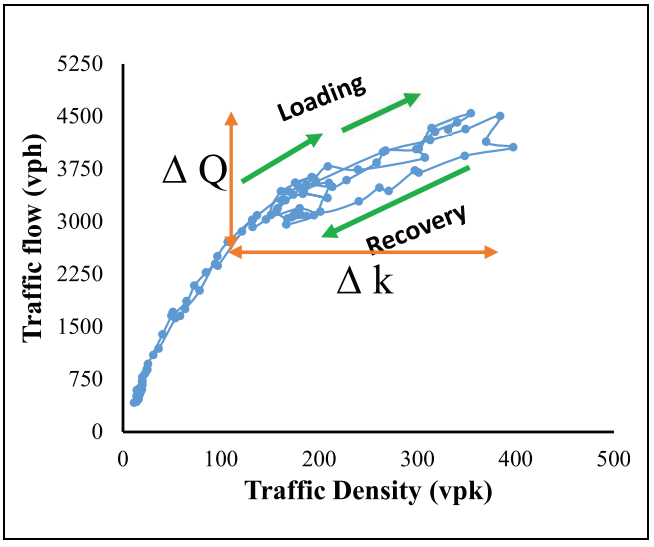

Figure 15. Flow–density relation and size of hysteresis loop.
Note: vph = vehicles per hour; vpk = vehicles per kilometer.

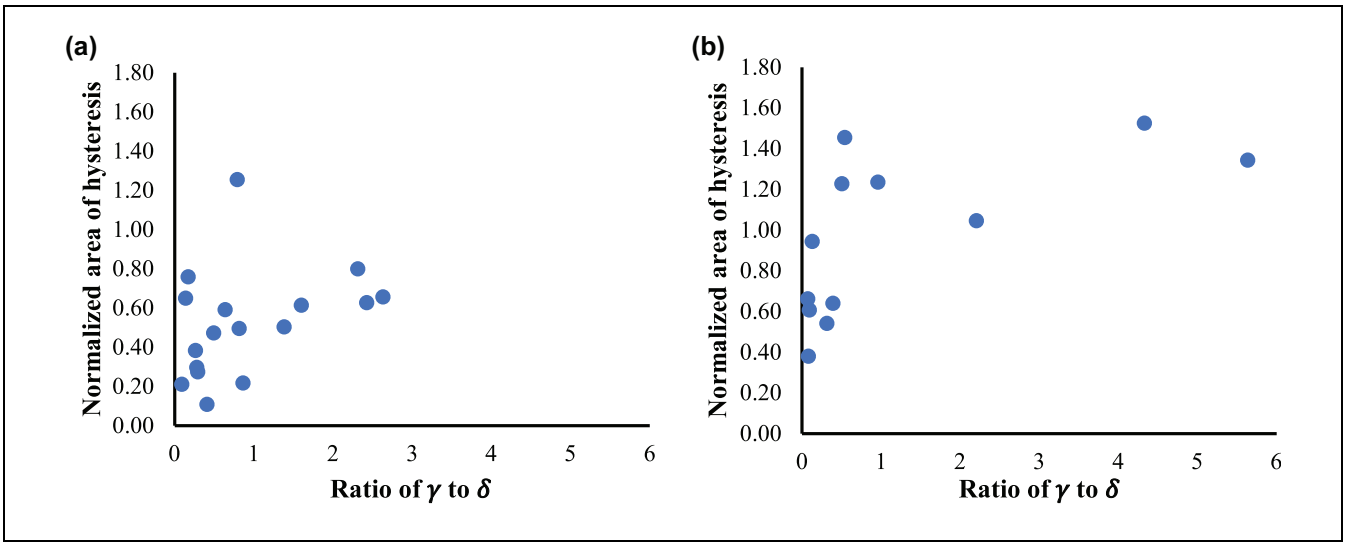

Figure 16. Variation in normalized area of hysteresis with ratio of γ to δ for: (*a*) empirical data and (*b*) simulated data.

Application of the MBPR Function

The application of the MBPR function is demonstrated by quantifying the impact of signal control through a before–after perspective. In response to increasing congestion levels, the local government authority installed a traffic signal control at 2nd Avenue in February 2018. Before that, the link FOB–Tidel had one signalized intersection at Tidel Park. For the present study, for the corridor (FOB–Tidel), the traffic signal control at 2nd Avenue was operational from February 2018. The signal is police controlled, and therefore, as per the perception of traffic police about the inflow, the cycle time is observed to vary. The traffic signal control installed at NI has an average cycle length of 120 s, with an average red time of 60 s. For the before case, travel time data were collected using Wi-Fi sensors for 3 days in November 2017.

The MBPR function was calibrated using the methodology discussed in the earlier sections. The calibrated MBPR link function for the before case is shown in Figure 17.

For similar values of traffic flow and TTU, travel time for the before and after case was computed using the calibrated MBPR function, and the results are illustrated in Figure 18.

From Figure 18, it can be concluded that for similar values of traffic flow and TTU, higher travel times can be noted for the before case compared with the after case. The statistical validation of this observation was performed by performing a one-way ANOVA at a 5% level of significance. The results of one-way ANOVA revealed a significant difference in travel time between the before and after cases. Compared with the before case, an average reduction of 13% in travel time was noted for the after case. Therefore, the installation of traffic signal control has reduced travel time and therefore reduced traffic congestion in the corridor.

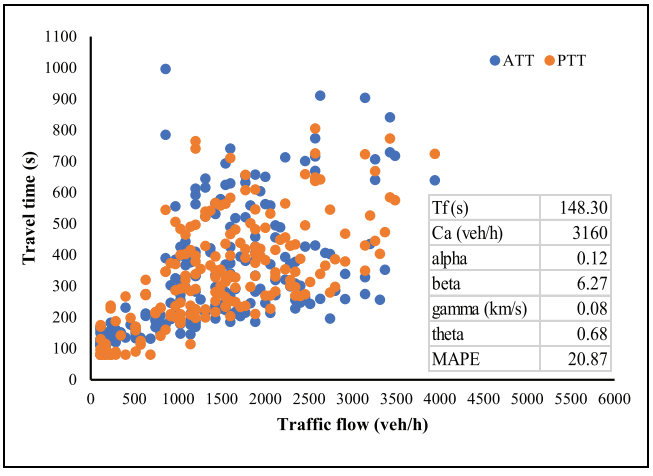

Figure 17. Calibrated MBPR function for the before case.
Note: MPBR = modified Bureau of Public Roads function; ATT = actual travel time; PTT = predicted travel time; MAPE = mean absolute percentage error; veh/h = vehicles per hour.

Conclusions and Way Forward

The BPR link function has profound application in transportation planning primarily because of its simple mathematical form, fewer and easily observable field inputs, and reasonable performance. However, the deterministic BPR function does not capture the stochastic relation between travel time and traffic flow and this forms its major limitation. The present study proposes a modified BPR link function by incorporating TTU in

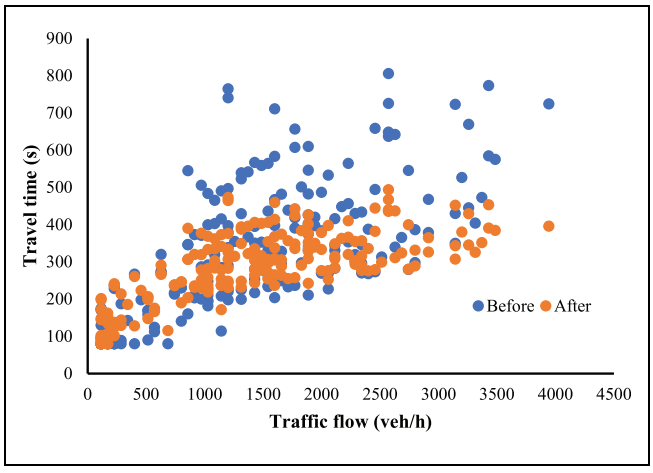

Figure 18. Travel time–traffic flow scatter for the before and after case.
Note: veh/h = vehicle per hour.

the existing BPR formulation. The effect of TTU is incorporated using two parameters, γ and δ. The applicability of the proposed MBPR function has been shown using empirical and simulated datasets. The following are some of the important conclusions drawn from the present study:

- TTU significantly affects travel time values in addition to traffic flow. The effect of TTU is pronounced during free-flow conditions. The TTU inherently captures the effect of changes in demand and supply (capacity).
- The MBPR function can replicate the stochastic relation between travel time and traffic flow better than the existing BPR function. Based on the value of TTU, for a given traffic flow, varying travel times are computed.
- The proposed MBPR function (a) captures the variability in travel time under oversaturated conditions and (b) captures the time-dependent relation between traffic volume and delay.
- The parameters of the MBPR function, namely γ and δ, have three critical physical interpretations as reflecting inter-day heterogeneity in travel times, infrastructure potential, and heterogeneity in the distribution of traffic flow.
- It is revealed that the ratio of γ to δ, when compared among links or between days for a given link, can explain the inter-day heterogeneity in travel times. A higher value of the γ to δ ratio indicates higher variability in travel times than does a smaller value of the γ to δ ratio.
- It is also exemplified that a higher ratio of γ to δ for a given value of Q, TTU, and α and β, generates higher travel time values than does a lower ratio of γ to δ, highlighting that the infrastructure is not effectively utilized.
- A higher ratio of γ to δ results in a higher value of the area of hysteresis, highlighting that traffic flow is heterogeneously distributed over a given value of density. Therefore, the values of the γ to δ ratio can be potentially used to analyze traffic flow stability.

The modified BPR function model was only checked for performance in the present study. The MBPR function can also be extended to traffic assignment problems and needs further investigation. TTU has a significant effect during free-flow conditions; therefore, characterizing traffic flow stability using density and TTU also forms the future scope of the study. The impact of different policies such as adaptive traffic signal control, vehicle segregation, and connected and autonomous vehicles can be studied using the values of γ and δ and also forms the future scope of the study. The application of MBPR for real-time or online studies needs further investigation.

Contribution of the Study

The present study proposes a stochastic extension of the deterministic BPR link cost function, referred to as the modified Bureau of Public Roads (MBPR) link cost function. The deterministic BPR function was converted into its stochastic version by integrating TTU. The TTU inherently incorporates the effect of changes in demand and supply (capacity). In the MBPR function, the effect of TTU is incorporated using two parameters, γ and δ. It is well articulated that traffic flow constantly transits from one traffic state to another. This variation in traffic states causes a variation in TTU and travel time values. The variation in TTU between different traffic states and over time periods is correlated, highlighting that TTU inherently entails the time-dependent nature of traffic flow. Because of this property of TTU, the MBPR function proposed in the present study (a) explains the stochastic nature of traffic flow, (b) represents the oversaturated conditions without the need for modified or oversaturated demand, and (c) explains the time-dependent relation between traffic flow and travel time. Therefore, the MBPR function proposed in the study significantly contributes to the existing literature.

Author Contributions

The authors confirm their contribution to the paper as follows: study conception and design: NG, SA, GJ, and CA; data collection: NG; analysis and interpretation of results: NG, SA, GJ, and CA; draft manuscript preparation: NG, SA, GJ, and CA. All authors reviewed the results and approved the final version of the manuscript.

Declaration of Conflicting Interests

The author(s) declared no potential conflicts of interest with respect to the research, authorship, and/or publication of this article.

Funding

The author(s) disclosed receipt of the following financial support for the research, authorship, and/or publication of this article: The authors would like to thank the Ministry of Housing and Urban Affairs (MoHUA), Government of India, which financially supported the research project entitled "Development of Framework for Measurement of Sustainability Index for Transportation System in Indian Metropolitan Cities" (File No. K-14011/18/2011-UT-IV (e)). The present study was part of this project. CA would like to acknowledge the "Joint Indo-German Center for Intelligent Transportation Systems–FuturTrans" project, funded by the BMBF (01DQ17018). SA would also acknowledge the TUM Global Visiting Professor Program, which facilitated the collaboration in this research.

ORCID iDs

Shriniwas Arkatkar https://orcid.org/0000-0002-1804-9465
Constantinos Antoniou https://orcid.org/0000-0003-0203-9542

References

1. Mtoi, E. T., and R. Moses. Calibration and Evaluation of Link Congestion Function: Applying Intrinsic Sensitivity of Link Speed as a Practical Consideration to Heterogeneous Facility Types within Urban Roads. *Journal of Transportation Technology*, Vol. 4, No. 2, 2014, pp. 141–149. http://doi.org/10.4236/jtts.2014.42014.
2. Das, A. K., and B. Rama Chilukuri. Link Cost Function and Link Capacity for Mixed Traffic Network. *Transportation Research Record: Journal of the Transportation Research Board*, 2020. 2674: 38–50.
3. Bureau of Public Roads. *Traffic Assignment Manual*. US Department of Commerce, Urban Planning Division, Washington, D.C., 1964.
4. Anwar, A. H. M. M., A. Fujiwara, and J. Zhang. Newly Developed Link Performance Functions Incorporating the Influence of On-Street Occupancy for Developing Cities: Study on Dhaka City of Bangladesh. TRB 90th Annual Meeting Compendium of Papers DVD, Washington, DC, 2011, p. 21.
5. Spiess, H. Technical Note—Conical Volume-Delay Functions. *Transportation Science*, Vol. 24, 1990, pp. 153–158.
6. Manzo, S., O. A. Nielsen, and C. G. Prato. Investigating Uncertainty in BPR Formula Parameters: A Case Study. *Proc., Strateg Forsk i Transp og infrastruktu, Danmarks Tekniske Universitet*, 2013.
7. Skabardonis, A., and R. Dowling. Improved Speed-Flow Relationships for Planning Applications. *Transportation Research Record: Journal of the Transportation Research Board*, 1997. 1572: 18–23.
8. Suh, S., C. H. Park, and T. J. A. Kim. Highway Capacity Function in Korea: Measurement and Calibration. *Transportation Research Part A: General*, Vol. 24, No. 3, 1990, pp. 177–186.
9. Huntsinger, L. F., and N. M. Rouphail. Bottleneck and Queuing Analysis: Calibration Volume-Delay Functions of Travel Demand Model. *Transportation Research Record: Journal of Transportation Research Board*, 2011. 2255: 117–124.
10. Wong, W., and S. C. Wong. Network Topological Effects on the Macroscopic Bureau of Public Roads Function. *Transportmetrica A: Transport Science*, Vol. 12, No. 3, 2016, pp. 272–296. http://doi.org/10.1080/23249935.2015.1129650.
11. García-Ródenas, R., and D. Verastegui-Rayo. Adjustment of the Link Travel-Time Functions in Traffic Equilibrium Assignment Models. *Transportmetrica A: Transport Science*, Vol. 9, No. 9, 2013, pp. 798–824. https://doi.org/10.1080/18128602.2012.669415.
12. Engelson, L. Properties of Expected Travel Cost Function with Uncertain Travel Time. *Transportation Research Record: Journal of Transportation Research Board*, 2011. 2254: 151–159.
13. Cetin, M., P. Foytic, S. Sun, A. J. Khattak, R. M. Robinson, and J. Lee. Calibration of Volume-Delay Functions for Traffic Assignment in Travel Demand Model. TRB 91st Annual Meeting Compendium of Papers DVD, Washington, DC, 2012, p. 14.
14. Foytik, P., M. Cetin, and R. M. Robinson. Calibration of BPR Function Based on Link Counts and Its Sensitivity to Varying Demand. TRB 92nd Annual Meeting Compendium of Papers, Washington, DC, 2013, p. 16.
15. Lam, W. H. K., and H. J. A. Huang. Combined Trip Distribution and Assignment Model for Multiple User Classes. *Transportation Research Part B: Methodological*, Vol. 26, No. 4, 1992, pp. 275–287.
16. Zhu, C., B. Jia, X. Li, and Z. Gao. A Stochastic Mixed Traffic Equilibrium Assignment Model Considering User Preferences. *Procedia-Social Behavioral Sciences*, Vol. 43, 2012, pp. 466–474.
17. Mesbah, M., M. Sarvi, and G. Currie. New Methodology for Optimizing Transit Priority at the Network Level. *Transportation Research Record: Journal of the Transportation Research Board*, 2008. 2089: 93–100.
18. Lien, J. W., V. V. Mazalov, A. V. Melnic, and J. Zheng. Wardrop Equilibrium for Networks with the BPR Latency Function. In *Discrete Optimization and Operations Research. DOOR 2016* (Y. Kochetov, Khachay, M., V. Beresnev, E. Nurminski, and P. Pardalos, eds.). Lecture Notes in Computer Science, LNCS 9869, Springer, Cham, Switzerland, 2016, pp. 37–49.
19. Godavarthi, G. R., R. S. Chalumuri, and S. Velmurugun. Measuring the Performance of Bus Rapid-Transit Corridors Based on Volume by Capacity Ratio. *Journals of Transportation Engineering*, Vol. 140, No. 10, 2014, p. 04014049. https://doi.org/10.1061/(ASCE)TE.1943-5436.0000698.

20. Anil, R., M. Satyakumar, and J. Jayakumar. Travel Time Estimation and Route for Emergency Vehicles under Indian Condition. *Proc., 3rd IEEE International Conference on Intelligent Transportation Engineering*, Singapore, IEEE, New York, October 3–5, 2018, pp. 247–252. https://doi.org/10.1109/ICITE.2018.8492696.
21. Pan, Y., J. Guo, and Y. Chen. Calibration of Dynamic Volume-Delay Functions: A Rolling Horizon-Based Parsimonious Modelling Perspective. *Transportation Research Record: Journal of Transportation Research Board*, 2022. 2676: 606–620.
22. Qiu, E., N. Virdi, H. Grzybowska, and T. Waller. Recalibration of the BPR Function for the Strategic Modelling of Connected and Autonomous Vehicles. *Transportmetrica B: Transport Dynamics*, Vol. 10, No. 1, 2022, pp. 779–800. https://doi.org/10.1080/21680566.2022.2040063.
23. Tu, H. *Monitoring Travel Time Reliability on Freeways*. TRAIL Thesis Series No. T2008/7. TRAIL Research School. The Netherlands, April 2008. http://resolver.tudelft.nl/uuid:9934cf45-7b77-411c-b030-8850a03a4bab
24. Tu, H., H. Li, H. van Lint, and H. van Zuylen. Modeling Travel Time Reliability of Freeways Using Risk Assessment Techniques. *Transportation Research Part A: Policy and Practice*, Vol. 46, No. 10, 2012, pp. 1528–1540.
25. Tu, H., J. W. C. Van Lint, and H. J. Van Zuylen. The Impact of Traffic Flow on Travel Time Variability of Freeway Corridors. *Transportation Research Record: Journal of Transportation Research Board*, 2007. 1993: 59–66.
26. Mahmassani, H. S., T. Hou, and M. Saberi. Connecting Networkwide Travel Time Reliability and the Network Fundamental Diagram of Traffic Flow. *Transportation Research Record: Journal of Transportation Research Board*, 2013. 2391: 80–91.
27. Yildirimoglu, M., Y. Limniati, and N. Geroliminis. Investigating Empirical Implications of Hysteresis in Day-to-Day Travel Time Variability. *Transportation Research Part C: Emerging Technologies*, Vol. 55, 2015, pp. 340–350. https://doi.org/10.1016/j.trc.2015.03.012.
28. Wang, H., D. Ni, Q. Y. Chen, and J. Li. Stochastic Modeling of the Equilibrium Speed-Density Relationship. *Journal of Advanced Transportation*, Vol. 47, 2013, pp. 126–150.
29. Qu, X., J. Zhang, and S. Wang. On the Stochastic Fundamental Diagram for Freeway Traffic: Model Development, Analytical Properties, Validation and Extensive Applications. *Transportation Research Part B: Methodological*, Vol. 104, 2017, pp. 256–271. https://doi.org/10.1016/j.trb.2017.07.003.
30. Ngoduy, D. Multiclass First Order Traffic Model Using Stochastic Fundamental Diagrams. *Transportmetrica*, Vol. 7, No. 2, 2011, pp. 111–125.
31. Li, J., Q. Y. Chen, H. Wang, and D. Ni. Analysis of LWR Model with Fundamental Diagram Subject to Uncertainties. *Transportmetrica*, Vol. 8, No. 6, 2012, pp. 387–405. https://doi.org/10.1080/18128602.2010.521532.
32. Knoop, V. L., and W. Daamen. Automatic Fitting Procedure for the Fundamental Diagram. *Transportmetrica B: Transport Dynamics*, Vol. 5, No. 2, 2016, pp. 129–144. https://doi.org/10.1080/21680566.2016.1256239.
33. Gore, N., S. S. Pulugurtha, S. Arkatkar, and G. Joshi. Congestion Index and Reliability Based Freeway Level of Service. *Journal of Transportation Engineering, Part A: Systems*, Vol. 147, No. 6, 2021, p. 04021027. https://doi.org/10.1061/JTEPBS.0000531.
34. Lu, W., J. Liu, J. Mao, G. Hu, C. Gao, and L. Liu. Macroscopic Fundamental Diagram Approach to Evaluating the Performance of Regional Traffic Controls. *Transportation Research Record: Journal of Transportation Research Board*, 2020. 2674: 420–430.
35. Brennan, T. M., J. M. Ernst, C. M. Day, D. M. Bullock, J. V. Krogmeier, and M. Martchouk. Influence of Vertical Sensor Placement on Data Collection Efficiency from Bluetooth MAC Address Collection Devices. *Journal of Transportation Engineering*, Vol. 136, No. 12, 2010, pp. 1104–1110.
36. Gore, N., S. Arkatkar, G. Joshi, and A. Bhaskar. Exploring Credentials of Wi-Fi Sensors as a Complementary Source of Transport Data: An Indian Experience. *IET Intelligent Transport Systems*, Vol. 13, No. 12, 2019, pp. 1860–1869. https://doi.org/10.1049/iet-its.2019.0251.
37. Porter, J. D., D. S. Kim, M. E. Magana, P. Poocharoen, and C. A. Gutierrez Arriaga. Antenna Characterization for Bluetooth-Based Travel Time Data Collection. *Journal of Intelligent Transportation Systems: Technology, Planning, and Operations*, Vol. 17, No. 2, 2013, pp. 142–151.
38. Singh, V., N. Gore, A. Chepuri, S. Arkatkar, G. Joshi, and S. Pulugurtha. Examining Travel Time Variability and Reliability on an Urban Arterial Road Using Wi-Fi Detections—A Case Study. *Journal of Eastern Asia Society for Transportation Studies*, Vol. 13, 2019, pp. 2390–2411. https://doi.org/10.11175/easts.13.2390.
39. PTV. *PTV VISSIM 9 User Manual*. PTV AG, 2016, p. 1055.
40. Arkatkar, S. S., and V. T. Arasan. Effect of Gradient and Its Length on Performance of Vehicles under Heterogeneous Traffic Conditions. *Journal of Transportation Engineering*, Vol. 136, No. 12, 2010, pp. 1120–1136.
41. Bhattacharyya, K., B. Maitra, and M. Boltze. Calibration of Micro-Simulation Model Parameters for Heterogeneous Traffic Using Mode-Specific Performance Measure. *Transportation Research Record:Journal of Transportation Research Board*, 2020. 2674: 135–147.
42. Chepuri, A., N. Raju, M. S. Bains, S. Arkatkar, and G. Joshi. Examining Performance of an Urban Corridor Using Microscopic Traffic Simulation Model under Mixed Traffic Environment in India. *Europei Transportei*, Vol. 69, 2018, pp. 1–21.
43. Paul, G., N. Raju, S. Arkatkar, and S. Easa. Can Segregating Vehicles in Mixed-Traffic Stream Improve Safety and Throughput? Implications Using Simulation. *Transportmetrica A: Transport Science*, Vol. 17, No. 4, 2021, pp. 1002–1026.
44. Nagle, A. S., and V. V. Gayah. Accuracy of Network-Wide Traffic States Estimated from Mobile Probe Data. *Transportation Research Record: Journal of Transportation Research Board*, 2014. 2421: 1–11.
45. Du, J., H. Rakha, and V. V. Gayah. Deriving Macroscopic Fundamental Diagrams from Probe Data: Issues and Proposed Solutions. *Transportation Research Part C: Emerging*

Technologies, Vol. 66, 2016, pp. 136–149. https://doi.org/10.1016/j.trc.2015.08.015.

46. Shim, J., J. Yeo, S. Lee, S. Hamdar, and K. Jang. Empirical Evaluation of Influential Factors on Bifurcation in Macroscopic Fundamental Diagram. *Transportation Research Part C: Emerging Technologies*, Vol. 102, 2019, pp. 509–520.
47. Tilg, G., S. Amini, and F. Busch. Evaluation of Analytical Approximation Methods for the Macroscopic Fundamental Diagram. *Transportation Research Part C: Emerging Technologies*, Vol. 114, 2020, pp. 1–19. https://doi.org/10.1016/j.trc.2020.02.003.
48. Gore, N., S. Arkatkar, G. Joshi, and A. Bhaskar. A Novel Methodology to Derive Vehicle Occupancy Using Wi-Fi Sensors under Heterogenous Traffic Conditions. Presented at the 98th Annual Meeting of Transportation Research Board, Washington, DC, 2019. https://trid.trb.org/view/1633208
49. Saberi, M., H. S. Mahmassani, T. Hou, and A. Zockaie. Estimating Network Fundamental Diagram Using Three-Dimensional Vehicle Trajectories: Extending Edie's Definitions of Traffic Flow Variables to Networks. *Transportation Research Record: Journal of Transportation Research Board*, 2014. 2422: 12–20.
50. Geroliminis, N., and C. Daganzo. Existence of Urban Scale Macroscopic Fundamental Diagram: Some Experimental Findings. *Transportation Research Part B: Methodological*, Vol. 42, 2008, pp. 759–770.
51. Wu, X., H. X. Liu, and N. Geroliminis. An Empirical Analysis on the Arterial Fundamental Diagram. *Transportation Research Part B: Methodological*, Vol. 45, 2011, pp. 255–266.
52. Dakic, I., and A. Stevanovic. On Development of Arterial Fundamental Diagrams Based on Surrogate Density Measures from Adaptive Traffic Control Systems Utilizing Stop-Line Detection. *Transportation Research Part C: Emerging Technologies*, Vol. 94, 2018, pp. 133–150. https://doi.org/10.1016/j.trc.2017.08.013.
53. Ambühl, L., A. Loder, M. C. J. Bliemer, M. Menendez, and K. W. Axhausen. A Functional Form with a Physical Meaning for the Macroscopic Fundamental Diagram. *Transportation Research Part B: Methodological*, Vol. 137, 2020, pp. 119–132. https://doi.org/10.1016/j.trb.2018.10.013.
54. Wong, W., S. C. Wong, and H. X. Liu. Network Topological Effects on the Macroscopic Fundamental Diagram. *Transportmetrica B: Transport Dynamics*, Vol. 9, No. 1, 2021, pp. 376–398. https://doi.org/10.1080/21680566.2020.1865850.
55. Thankappan, A., and L. Vanajakshi. Development and Application of a Traffic Stream Model under Heterogeneous Traffic Conditions. *Journal of Institution of Engineers (India): Series A*, Vol. 96, No. 4, 2015, pp. 267–275. https://doi.org/10.1007/s40030-015-0134-y.
56. Saberi, M., and H. Mahmassani. Hysteresis and Capacity Drop Phenomena in Freeway Networks: Empirical Characterization and Interpretation. *Transportation Research Record: Journal of Transportation Research Board*, 2013. 2391: 44–55.